Title
Improvement of 3D Printing Resolution by the Development of Shrinkable Materials

Author
Chia, Helena

Publication Date
2014

Peer reviewed|Thesis/dissertation

UNIVERSITY OF CALIFORNIA

Los Angeles

Improvement of 3D Printing Resolution by the Development of Shrinkable Materials

A dissertation submitted in partial satisfaction of the requirements for the degree Doctor of Philosophy in Biomedical Engineering

by

Helena Nien-Hwa Chia

2014

ABSTRACT OF THE DISSERATION

Improvement of 3D Printing Resolution by the

Development of Shrinkable Materials

by

Helena Nien-Hwa Chia

Doctor of Philosophy in Biomedical Engineering

University of California, Los Angeles, 2014

Professor Benjamin Wu, Chair

Three-dimensional printing (3DP) uses inkjet printheads to selectively deposit liquid binder to adjoin powder particles in a layer-by-layer fashion to create a computer-modeled 3D object. Two general approaches for 3DP have been described for biomedical applications-- direct and indirect 3DP. The two approaches offer competing advantages, and both are limited by print resolution. This study describes materials processing strategies to enhance both indirect and direct 3DP resolution by shrinking.

For indirect 3DP, 3DP resolution was improved by controlled shrinking of net-shape scaffolds. Briefly, porogen preforms are printed and infused with the desired monomer or polymer solution. After solidification or polymerization, the porogen is leached and the polymer is allowed to shrink by controlled drying. Heat treatment is performed to retain the dimensions against swelling forces. The main objectives are to determine the effects of polymer content and

post-processing on dimension, microstructure, and thermomechanical properties of the scaffold. For polyethylene glycol diacrylate, reducing polymer content corresponded with greater shrinkage, with maximum shrinkage of ~80 vol% at polymer content of 20%. The secondary heat treatment retains the microarchitecture and new dimensions of the scaffolds, even when the scaffolds are immersed into water. This material processing strategy provides an alternative method to enhance the resolution of 3D scaffolds, for a wide range of polymers, without optimizing the binder-powder interaction physics for each material combination.

For direct 3DP, a novel fabrication method was developed to create prints without organic solvent in the binder and shrinking was induced by a solvent plasticizer. PLGA was first made into microparticles and then mixed with sucrose particles to create the printing powder. A water-based binder was deposited onto the powder layers to create a print and then the polymer microparticles fused together with solvent vapor fusion. The sucrose was then removed by leaching and PLGA scaffolds permanently shrunken ~80% volumetrically in a solution of methanol to a final resolution of ~400 μm. The methanol was acting as a plasticizer by decreasing the T_g below room temperature to allow for the polymer network to collapse upon itself. This approach to increasing the resolution allows for material flexibility of 3DP by increasing the range of materials used in this process since polymer microparticles are fused after printing and polymer-binder printing conditions do not need to be optimized.

This thesis presents novel materials processing strategies to improve the resolution of indirect and direct 3DP resolution for biomaterials.

This dissertation of Helena Nien-Hwa Chia is approved by:

Chih-Ming Ho

James Dunn

Min Lee

Benjamin Wu, Committee Chair

UNIVERSITY OF CALIFORNIA, LOS ANGELES

2014

TABLE OF CONTENTS

LIST OF FIGURES

CHAPTER 2

CHAPTER 3

LIST OF TABLES

ACKNOWLEDGEMENTS

I would like to thank my advisor, Professor Ben Wu, for this opportunity and his help. I am extremely grateful to have such a great advisor who leads a collaborative lab. I appreciate his investment of time and resources into my project and me. I've learned a lot about 3D printing and myself in this process and Dr. Wu has been a true mentor to me.

I would also like to thank my committee members of Professors Chih-Ming Ho, James Dunn, and Min Lee. Their suggestions have made my research better and I am grateful for their time and support.

I would like to acknowledge people who have helped me throughout the UCLA campus. For materials characterization, Dr. Sergey Pridhiko and Dr. Ignacio Martini have helped train me and answer any questions I have. I would also like to thank Dr. Jinny Kwak and Dr. Kang Ting for assistance and use of μ-CT. The Bioengineering staff of Apryl Chin, Stacey Fong, Anne-Marie Dieters, Brian Lee, and Larry Nadeau has really been great and I appreciate all their help.

I would like to acknowledge my labmates and thank them for never hesitating to help or chat. I'm very lucky to work with Abigail Parks, Chase Linsley, Eric Tsang, Stephanie Reed, Cheng-Han Chen, Arnold Suwarnasarn, Chris Walthers, and Yulong Zhang.

I would also like to acknowledge my friends and family who have made my life fun and fulfilled. The support of Tim, Josie and Rebecca Rhee is infinite and I thank them for that. Ken Lin, my snack buddy, and Minna Ha have been just amazing friends and I'm so glad to have them in my life. Pradeep Senanayake has been a great partner-in-crime for my time at UCLA and I'm lucky to have shared this experience with him.

Lastly, my parents have been steadfast in their encouragement and support all these years. Through the ups and downs they always encouraged me and I feel really fortunate to have that kind of support.

VITA

2004	B.S. Mechanical Engineering MIT, Cambridge, MA
2006	M.S. Biomedical Engineering University of California, Davis
2007	M.S. Biomedical Engineering University of California, Los Angeles
2006-2013	Teaching Assistant Biomedical Engineering University of California, Los Angeles
2008-2010	NSF Materials Creation Training Program Fellow
2010	Summer Research Intern Materials Science and Engineering Imperial College of London

CHAPTER 1: INTRODUCTION

1.1 Background

1.1.1 Computer-aided Tissue Engineering

When making biomedical devices, the design of the architecture on the macro, micro, and nano level is important. The macroarchitecture is the overall shape of the device which can be complex (e.g. patient and organ specificity, anatomical features), the microarchitecture reflects the tissue architecture (e.g. pore size, shape, porosity, spatial distribution, and pore interconnection), and the nanoarchitecture is surface modification (e.g. biomolecule attachment for cell adhesion, proliferation, and differentiation). Common techniques to produce porosity and a range of pores size are gas foaming, solvent casting with particle leaching, freeze-drying, and eletrospinning. While the microarchitecture in these methods is well-controlled and understood, the ability to control macroarchitecture with these methods is limited to shapes and geometries determined by molds and manual processing. The ability to incorporate internal architecture or curved channels is also limited when using these methods.

Computer-aided tissue engineering has allowed for the design and fabrication of complex 3D structures which can be patient specific. The integration of computer aided design, advanced imaging techniques (i.e. magnetic resonance imaging and computer tomography), and rapid prototyping has advanced fabrication of objects with both macro and microarchitecture control. In addition, patient specific imaging can be used to customize builds for individuals [1, 2]. A type of rapid prototyping, solid free form fabrication (SFF), offers a method to control both the micro and macroarchitecture to create complex biomedical devices from computer-aided tissue engineering.

1.1.2 Solid Freeform Fabrication for Biomedical Devices

SFF methods build 3D biomedical devices in a layer-by-layer process. The general SFF process is 1) creating a 3D computer model (can be generated from medical imaging data such as CT scans or X-rays) 2) slicing the 3D computer model into a build file of 2D images with software, 3) fabricating the build by a computer-controlled layer-by-layer process, and 4) finishing with any post processing such as surface modification for nanoarchitecture. Particular advantages of SFF are 1) the ability to design highly-complex parts on CAD (e.g. patient specific parts, overhangs and undercuts, internal volumes), 2) computer-controlled fabrication allowing for controlled adjustment of process parameters, 3) control over local pore morphology and porosities in the same scaffold, and 4) a range of processing conditions. The SFF technologies briefly reviewed below are 3D printing (3DP), fused deposition modeling (FDM), stereolithography (SLA), selective laser sintering (SLS), and bioplotting.

1.1.3 3D Printing

Three-dimensional printing (3DP) was developed at Massachusetts Institute of Technology [3-5]. Loose powder particles are spread in a thin layer. Selective deposition of liquid binder from an inkjet printhead creates a 2D pattern of bound particles. This process is repeated layer by layer until a 3D object is built. Parts are removed from the powder bed and unbound powder is removed. Since objects are supported by the surrounding unbound powder, this technique allows for scaffolds with channels or overhang features. Direct 3DP produces the final part composed of the powder and binder used in fabrication. Materials used in direct 3DP include powder composed of a synthetic polymer (i.e. poly (ε-caprolactone), polylactide–coglycolide or poly (L-lactic acid)) with organic solvent as binder [5-7] and natural polymer powder (i.e.starch, dextran

and gelatin) with water as binder [8, 9]. Indirect 3DP prints a mold which is then cast with the final polymer and porogen materials. Materials used in indirect 3DP to print the mold include commercially available plaster powder (i.e. calcium sulfate hemihydrate plaster powder) and water-based binder. The mold is then cast with a slurry of biodegradable polymer dissolved in solvent mixed with porogen (i.e.polylactide–coglycolide in chloroform mixed with NaCl) [10, 11].

An advantage of direct 3DP is direct control over both the microarchitecture (i.e. pore size) and macroarchitecture (i.e. overall shape). Prints which use porogen as the powder result in high pore interconnectivity, uniform porosity, and defined pore size after leaching. This method has shown to fabricate scaffolds which can support hepatocyte ingrowth [6]. Unlike indirect 3DP, there are no limitations on the macroarchitecture and no need for demolding. One limitation of direct 3DP is that organic solvents can dissolve polymers used in most printheads. To overcome this limitation, investigators used stencils to pattern polymer solutions onto porogen particles (NaCl) to fabricate scaffolds [6]. However, the use of stencils prevents fabrication of highly complex shapes or small features. Organic solvent-compatible, high precision printheads are available but they are optimized for a narrow range of polymeric solutions. Another limitation of direct 3DP is that layer thickness must be greater than porogen particle size, and less than 150 μm maximum threshold to maintain interlayer connectivity and part strength during printing [12]. To overcome this porogen size limitation, larger pores must be printed.

Indirect 3DP overcomes many of the limitations of direct 3DP. The use of aqueous binder allows the use of consumer grade inkjet printheads, and eliminates the need for stencils [10]. A negative mold is printed using commercially available plaster powder and then cast with

the desired porogen dispersed in a polymer solution. The porogen size is not limited since it does not affect printing resolution or layer interconnectivity. High materials flexibility with polymer-porogen combinations is possible due to independence from powder material properties. This method can be used to create small, high aspect ratio features (i.e. small intestine villi) or large scale, highly porous scaffolds (i.e. anatomically shaped zygoma scaffolds with pore sizes 300-500 μm) [11]. The limitations of indirect 3DP are 1) challenges in uniform, high density packing of porogen in complex features (i.e. intricate internal undercuts or intersecting channels) and 2) restrictions on shape or feature design due to difficulty demolding. Incomplete packing will result in loss of uniform microarchitecture and desired macroarchitecture.

The key advantages of 3DP are the wide range of materials able to be used due to room temperature processing and the material used in powder form, ability to print overhangs and internal architecture, and microstructure control. The disadvantages of 3D printing are the limited use of organic solvents as binders due to dissolving of commercial printheads and difficulty in removing unbound powder from small or curved channels.

1.1.4 Fused Deposition Modeling

Fused deposition modeling (FDM) is the deposition of molten material through an extrusion head with a small orifice in a specific laydown pattern. To create overhanging features, a removable supporting structure can also be deposited during the process. Thermoplastics such as ABS are commonly used due to their low melting points but for bioapplications PCL is commonly used due to its low melting temperature of ~60°C, low glass transition temperature of -60°C, and high thermal stability [13-15]. Recently, PLGA has been used with FDM to create scaffolds, however, the high glass transition temperature of PLGA (40-60°C) makes processing

PLGA challenging with a higher extrusion temperature required [15-17]. The material is heated to ~110-140°C to create the right material flow properties for extrusion from the nozzle and fusion of the layers [13, 14, 16, 17]. Materials can also be combined in this technology such as poly(ethylene glycol) terephthalate and poly(butylene terephthalate) or polypropylene and tricalcium phosphate [18, 19]. Controllable variables are raster thickness, raster gap width (space between rasters), raster angle, and layer thickness (dependent on extrusion tip diameter).

The key advantages of FDM is high porosity due to the laydown pattern and good mechanical strength. The disadvantages of FDM are the limited materials which when molten have high enough viscosity to build but low enough to extrude, the inability to incorporate cells or growth factors due to the high processing temperature, and need for a secondary structure to support overhangs.

1.1.5 Stereolithography

SLA was developed in the late 1980s and is based on spatially controlled solidification of a liquid resin by photopolymerization. A laser beam (UV) or a digital light projector scans the surface of a pool of liquid photocurable polymer to solidify the cross-section. The platform then lowers in the bottom-up approach and another liquid layer of polymer covers the solidified build for the next layer of polymerized material. For the top-down approach, light is projected on a transparent plate on the bottom of the vessel holding the liquid resin for building each layer. The build must be separated from the plate to add each additional layer. The depth of the platform is controlled so that the layers are adhered together during the layer-by-layer building. When the structure is completed, the unpolymerized liquid resin is removed by draining and post-curing converts any unreacted groups.

Kinetics of the curing reactions occurring during polymerization is critical. This affects the curing time and the thickness of the layer polymerized. The kinetics can be controlled by the power of the light source, the scanning speed and the chemistry and amount of the monomer and photointiators. In addition, UV absorbers can be added to the resin to control the depth of polymerization [20].

The materials used with SLA are limited due to those that are photocrosslinkable such as poly(propylene fumarate) [21] and PEG dimethacrylate [22]. SLA has also moved toward using biodegradable materials by synthesizing new polymers such as PDLLA-PEG-PDLLA-based macromers [23]. Macromers with higher molecular weights or glass transition temperatures require a diluent to reduce the viscosity of the resin such as water or N-methylpyrrolidone.

Stereolithography has moved toward encapsulation of cells during polymerization in hydrogels. Studies have shown the ability to encapsulate cells during stereolithography but there are limitations. First, the resin must be water-based and studies using PBS and HEPES buffer as the main component have seen sacrifices of resolution to 250 μm resolution in the x-y plane and 150-250 μm layer resolution [24, 25]. The parts produced from the studies have a minimum of 1 mm dimension for features. The second main limitation is the cytotoxicity of the initiator and UV exposure. A build with a multiple layers will require more time exposed to these conditions and is limited by the time of polymerization for each layer. Lastly, most likely due to the low mechanical stiffness of the hydrogels, there is a lack of macropores designed into the build as is commonly seen with SLA.

The advantage is the ability to create complex shapes with internal architecture, good mechanical strength, and high feature resolution (~1.2 um) [26]. The disadvantages are the need to use materials which are photocurable, which include use of photointiators and radicals, long

processing times for large builds, entrapment of unreacted monomer and residual photoinitiator, and inability to use more than one resin at a time.

1.1.6 Selective Laser Sintering

SLS is similar to 3D printing except a laser beam scans the surface of the powder for each layer to fuse together particles heated above the glass transition temperature. The resolution of features is determined by powder particle size, focused laser beam diameter and heat transfer in the powder bed. The limit to particle size is 10 um due to poor spreading and sintering too quickly causing edge inaccuracies. Materials commonly used are PCL and a combination of polyether ether ketone and hydroxyapatite [27-30]. With biomaterials, thin solid disks are commonly made but feature are made on the ~400-500 μm scale.

The key advantages of SLS is the lack of use of organic solvent or a filament, control of internal architectures and porosity, and ease of incorporation of multiple materials. The main disadvantages are limited materials which fuse but do not decompose under the laser beam (high temperatures) and the post processing needed to remove trapped powder.

1.1.7 3D Plotting and Bioplotting

3D plotting extrudes a viscous liquid material (i.e. solution or paste) deposited in one long continuous strand or in individual dots from a nozzle or syringe to create a desired 3D shape of ceramics, polymers, or hydrogels [31]. The process can be at room temperature or at elevated temperatures. For example, thermoreversible natural polymers such as agar and gelatin in solution are heated and extruded at ~80°C into a cooler liquid medium (~20°C) [32, 33]. Another approach is to extrude polymers into a liquid medium containing reactants for

crosslinking. An example material is extruding gelatin into a Ca^{2+} reservoir for microvasculature [34]. For other materials such as tricalcium phosphate, a solution is made with water, extruded from a syringe, and then lyophilized to remove the liquid[35]. The resulting diameter of each strut was ~400 μm.

3D bioplotting is the incorporation of cells directly into the hydrogel structures during the fabrication process. Example applications are rat smooth muscle cell-laden collagen droplets (650 μm diameter) to create specific cell spatial patterns in 3D [36].

This SFF method is especially good for low viscosity materials and the buoyancy due to the density matching of the extruded material to the liquid medium prevents collapse of the shape. The strand thickness can be varied by material viscosity, deposition speed, extrusion tip diameter, and applied pressure.

The key advantages of bioplotting are the room temperature processing (if applicable) and direct incorporation of cells. The key disadvantages are limited mechanical stiffness, critical timing of gelation time, specific matching of material and liquid medium densities to preserve shapes, and low resolution.

1.1.8 Selection of 3DP

The key advantages of 3D printing (3DP), over other SFF methods, are 1) material flexibility due to room temperature processing and material in powder form, 2) control of the micro and macroarchitecture, and 3) porogens can be used for the build. Therefore, 3DP will be used as the SFF method in this work.

The Wu Lab currently has projects developing binder with increased resolution and strength by the addition of polyacrylic acid to the binder solution and a thin layer of oil between

powder layers, spray-drying spherical powder to facilitate removal of trapped powder, and creating unidirectional, interconnected pores by the control of a freezing front. The best resolution for water-soluble porogen (sucrose) able to be printed in this lab is ~1 mm.

1.1.9 Resolution Needs

Spatial resolution is extremely important-- how small do the features have to be? Anatomical features and tissue architecture may have details on the scale of hundreds of microns (e.g. villi of the small intestine with ~500 um diameters and 1 mm length). Diffusion consumption modeling has shown a 200 um limit in scaffolds for oxygen transport to cells, resulting in a maximum of 400 um diameter features for cell survival [37]. Therefore, the current resolution of ~1 mm for sugar and water-soluble powders must be improved ~50% while maintaining material flexibility.

1.1.10 Resolution Limitations and Strategies

The main constraint on resolution for 3DP is the physical deformation of liquid droplet binders onto solid particles during ballistic impact at the moment of liquid-solid contact, and the subsequent capillary drawing of the liquid binder away from the target zone into nearby empty pores between the dry powder particles (Batten, 1984). An example is the bleeding of the binder adding 150 μm to the dimensions of a printed feature designed 300-700 μm [10].

One strategy is to retard the migration of the binder by 1) increasing the contact angle of the binder and powder and surface tension and 2) increasing the particle size of the powder to reduce permeability. However, any changes must still enable the binder to be deposited from printer nozzles, lamination of the layers, spreading of the powder, and good resolution.

Previously in the Wu lab, the printing resolution of water-soluble porogen (sucrose) has been improved to ~1 mm by adding a thin hydrophobic layer on top of each sucrose layer before binder deposition, optimization of the sucrose particle size, and optimization of the binder composition (Phil and Armen). The water-soluble porogen print would then be used as a preform, with the polymer of interest infiltrated and sucrose removed by leaching to create a scaffold.

Another strategy is to take the optimized printing conditions and to increase resolution by shrinking. For an indirect 3DP approach, a water-soluble print can be used as a preform. The polymer of choice is infiltrated into the preform, the polymer crosslinked, and the sucrose removed by leaching. For a direct 3DP approach, the polymer of choice is incorporated into the print and directly shrunken. The goal of this work is to increase printing resolution with this strategy since it can be applied to future improved printing conditions.

1.2 Research Objectives

To reach the desired resolution of ~400-500 μm, an increase in the spatial resolution is needed. While fabrication methods can be further studied to improve resolution, another approach to increasing feature resolution is to shrink either the infiltrate, or the original print. In the former case, the printed preform is infiltrated by a material that is capable of shrinking. In the latter case, the print is directly treated to shrink. The objective of this project is to develop general strategies for each approach. The aims are:

Aim 1: To develop a materials processing strategy to increase indirect 3DP resolution.

Aim 2: To develop a materials processing strategy to increase direct 3DP resolution.

References

[1] Winder J, Bibb R. Medical rapid prototyping technologies: state of the art and current limitations for application in oral and maxillofacial surgery. Journal of Oral and Maxillofacial Surgery. 2005;63:1006-15.

[2] Colin A, Boire J-Y. A novel tool for rapid prototyping and development of simple 3D medical image processing applications on PCs. Computer methods and programs in biomedicine. 1997;53:87-92.

[3] Cima MJ, Sachs E, Cima LG, Yoo J, Khanuja S, Borland SW, et al. Computer-derived microstructures by 3D printing: bio-and structural materials. Solid Freeform Fabr Symp Proc: DTIC Document; 1994. p. 181-90.

[4] Griffith LG, Wu B, Cima MJ, Powers MJ, Chaignaud B, Vacanti JP. In Vitro Organogenesis of Liver Tissuea. Annals of the New York Academy of Sciences. 1997;831:382-97.

[5] Wu BM, Borland SW, Giordano RA, Cima LG, Sachs EM, Cima MJ. Solid free-form fabrication of drug delivery devices. Journal of Controlled Release. 1996;40:77-87.

[6] Kim SS, Utsunomiya H, Koski JA, Wu BM, Cima MJ, Sohn J, et al. Survival and function of hepatocytes on a novel three-dimensional synthetic biodegradable polymer scaffold with an intrinsic network of channels. Annals of surgery. 1998;228:8.

[7] Zeltinger J, Sherwood JK, Graham DA, Müeller R, Griffith LG. Effect of pore size and void fraction on cellular adhesion, proliferation, and matrix deposition. Tissue Engineering. 2001;7:557-72.

[8] Lam CXF, Mo XM, Teoh SH, Hutmacher DW. Scaffold development using 3D printing with a starch-based polymer. Materials Science and Engineering: C. 2002;20:49-56.

[9] Seitz H, Rieder W, Irsen S, Leukers B, Tille C. Three-dimensional printing of porous ceramic scaffolds for bone tissue engineering. Journal of Biomedical Materials Research Part B: Applied Biomaterials. 2005;74:782-8.

[10] Lee M, Dunn JCY, Wu BM. Scaffold fabrication by indirect three-dimensional printing. Biomaterials. 2005;26:4281-9.

[11] Lee M, Wu BM, Dunn JCY. Effect of scaffold architecture and pore size on smooth muscle cell growth. Journal of Biomedical Materials Research Part A. 2008;87:1010-6.

[12] Wu BM, Cima MJ. Effects of solvent-particle interaction kinetics on microstructure formation during three-dimensional printing. Polymer Engineering & Science. 1999;39:249-60.

[13] Zein I, Hutmacher DW, Tan KC, Teoh SH. Fused deposition modeling of novel scaffold architectures for tissue engineering applications. Biomaterials. 2002;23:1169-85.

[14] Hutmacher DW, Schantz T, Zein I, Ng KW, Teoh SH, Tan KC. Mechanical properties and cell cultural response of polycaprolactone scaffolds designed and fabricated via fused deposition modeling. Journal of biomedical materials research. 2001;55:203-16.

[15] Suggs LJ, Moore SA, Mikos AG. Synthetic biodegradable polymers for medical applications. Physical properties of polymers handbook: Springer; 2007. p. 939-50.

[16] Park SH, Park DS, Shin JW, Kang YG, Kim HK, Yoon TR, et al. Scaffolds for bone tissue engineering fabricated from two different materials by the rapid prototyping technique: PCL versus PLGA. Journal of Materials Science: Materials in Medicine. 2012;23:2671-8.

[17] Kim J, McBride S, Tellis B, Alvarez-Urena P, Song Y-H, Dean DD, et al. Rapid-prototyped PLGA/β-TCP/hydroxyapatite nanocomposite scaffolds in a rabbit femoral defect model. Biofabrication. 2012;4:025003.

[18] Woodfield TB, Malda J, De Wijn J, Peters F, Riesle J, van Blitterswijk CA. Design of porous scaffolds for cartilage tissue engineering using a three-dimensional fiber-deposition technique. Biomaterials. 2004;25:4149-61.

[19] Kalita SJ, Bose S, Hosick HL, Bandyopadhyay A. Development of controlled porosity polymer-ceramic composite scaffolds via fused deposition modeling. Materials Science and Engineering: C. 2003;23:611-20.

[20] Heller C, Schwentenwein M, Russmueller G, Varga F, Stampfl J, Liska R. Vinyl esters: low cytotoxicity monomers for the fabrication of biocompatible 3D scaffolds by lithography based additive manufacturing. Journal of Polymer Science Part A: Polymer Chemistry. 2009;47:6941-54.

[21] Lee K-W, Wang S, Fox BC, Ritman EL, Yaszemski MJ, Lu L. Poly (propylene fumarate) bone tissue engineering scaffold fabrication using stereolithography: effects of resin formulations and laser parameters. Biomacromolecules. 2007;8:1077-84.

[22] Mapili G, Lu Y, Chen S, Roy K. Laser-layered microfabrication of spatially patterned functionalized tissue-engineering scaffolds. Journal of Biomedical Materials Research Part B: Applied Biomaterials. 2005;75:414-24.

[23] Seck TM, Melchels FP, Feijen J, Grijpma DW. Designed biodegradable hydrogel structures prepared by stereolithography using poly (ethylene glycol)/poly (d, l-lactide)-based resins. Journal of Controlled Release. 2010;148:34-41.

[24] Dhariwala B, Hunt E, Boland T. Rapid prototyping of tissue-engineering constructs, using photopolymerizable hydrogels and stereolithography. Tissue engineering. 2004;10:1316-22.

[25] Arcaute K, Mann BK, Wicker RB. Stereolithography of three-dimensional bioactive poly (ethylene glycol) constructs with encapsulated cells. Annals of biomedical engineering. 2006;34:1429-41.

[26] Zhang X, Jiang X, Sun C. Micro-stereolithography of polymeric and ceramic microstructures. Sensors and Actuators A: Physical. 1999;77:149-56.

[27] Lohfeld S, Tyndyk M, Cahill S, Flaherty N, Barron V, McHugh P. A method to fabricate small features on scaffolds for tissue engineering via selective laser sintering. J Biomed Sci Eng. 2010;3:138-47.

[28] Yeong WY, Sudarmadji N, Yu HY, Chua CK, Leong KF, Venkatraman SS, et al. Porous polycaprolactone scaffold for cardiac tissue engineering fabricated by selective laser sintering. Acta biomaterialia. 2010;6:2028-34.

[29] Wiria FE, Leong KF, Chua CK, Liu Y. Poly-< i> ε</i>-caprolactone/hydroxyapatite for tissue engineering scaffold fabrication via selective laser sintering. Acta Biomaterialia. 2007;3:1-12.

[30] Tan K, Chua C, Leong K, Cheah C, Cheang P, Abu Bakar M, et al. Scaffold development using selective laser sintering of polyetheretherketone–hydroxyapatite biocomposite blends. Biomaterials. 2003;24:3115-23.

[31] Landers R, Mülhaupt R. Desktop manufacturing of complex objects, prototypes and biomedical scaffolds by means of computer-assisted design combined with computer-guided 3D plotting of polymers and reactive oligomers. Macromolecular Materials and Engineering. 2000;282:17-21.

[32] Landers R, Hübner U, Schmelzeisen R, Mülhaupt R. Rapid prototyping of scaffolds derived from thermoreversible hydrogels and tailored for applications in tissue engineering. Biomaterials. 2002;23:4437-47.

[33] Maher P, Keatch R, Donnelly K, Paxton J. Formed 3D bio-scaffolds via rapid prototyping technology. 4th European Conference of the International Federation for Medical and Biological Engineering: Springer; 2009. p. 2200-4.

[34] Pataky K, Braschler T, Negro A, Renaud P, Lutolf MP, Brugger J. Microdrop Printing of Hydrogel Bioinks into 3D Tissue-Like Geometries. Advanced Materials. 2012;24:391-6.

[35] Haberstroh K, Ritter K, Kuschnierz J, Bormann KH, Kaps C, Carvalho C, et al. Bone repair by cell-seeded 3D-bioplotted composite scaffolds made of collagen treated tricalciumphosphate or tricalciumphosphate-chitosan-collagen hydrogel or PLGA in ovine critical-sized calvarial defects. Journal of Biomedical Materials Research Part B: Applied Biomaterials. 2010;93:520-30.

[36] Moon S, Hasan SK, Song YS, Xu F, Keles HO, Manzur F, et al. Layer by layer three-dimensional tissue epitaxy by cell-laden hydrogel droplets. Tissue Engineering Part C: Methods. 2009;16:157-66.

[37] Dunn JCY, Chan WY, Cristini V, Kim JS, Lowengrub J, Singh S, et al. Analysis of cell growth in three-dimensional scaffolds. Tissue engineering. 2006;12:705-16.

CHAPTER 2: IMPROVED RESOLUTION OF INDIRECT 3D PRINTED SCAFFOLDS BY SHRINKING

2.1 Introduction

Indirect 3DP prints a mold which is then cast with the final polymer and porogen materials. Materials used in indirect 3DP to print the mold include commercially available plaster powder (i.e. calcium sulfate hemihydrate plaster powder) and water-based binder. The mold is then cast with a slurry of biodegradable polymer dissolved in solvent mixed with porogen (i.e.polylactide–coglycolide in chloroform mixed with NaCl) [1, 2].

Indirect 3DP overcomes many of the limitations of direct 3DP. The use of aqueous binder allows the use of consumer grade inkjet printheads, and eliminates the need for stencils [1]. A negative mold is printed using commercially available plaster powder and then cast with the desired porogen dispersed in a polymer solution. The porogen size is not limited since it does not affect printing resolution or layer interconnectivity. High materials flexibility with polymer-porogen combinations is possible due to independence from powder material properties. This method can be used to create small, high aspect ratio features (i.e. small intestine villi) or large scale, highly porous scaffolds (i.e. anatomically shaped zygoma scaffolds with pore sizes 300-500 μm) [2]. The limitations of indirect 3DP are 1) challenges in uniform, high density packing of porogen in complex features (i.e. intricate internal undercuts or intersecting channels) and 2) restrictions on shape or feature design due to difficulty demolding. Incomplete packing will result in loss of uniform microarchitecture and desired macroarchitecture.

Another approach to using indirect 3DP is to first print a preform, infiltrate the desired material and crosslink, and then remove the original printing powder by leaching. A sacrificial material can be used to coat the preform first due to compatibility. This approach reduces the limitations of shapes due to mold removal. In addition, since a porogen can be used as printing

powder, final parts would have uniform, high density packing of porogen. The use of a preform has been demonstrated previously in the lab with sucrose as the porogen printing powder and PCL as the final material [3]. Also, gelatin has been used as the porogen printing powder, infiltrated with a sacrificial material of PCL, and then the final material of chitosan added [4]. The resolution reached for both studies is ~1mm due to lateral migration of the binder even with optimized binder composition, binder viscosity, and particle size of the powder.

An approach to improve indirect 3DP resolution is by shrinking. The process is overviewed in Figure 1. Briefly, an aqueous binder is patterned onto a porogen powder (i.e. sucrose) in a layer-by-layer fashion to create a 3DP composed entirely of porogen (preform). The interstitial spaces between porogen particles of the preform are infiltrated with the desired monomer or polymer solution. The monomer or polymer is then polymerized and the porogen is removed by leaching to produce a polymer scaffold with original preform shape (net-shape scaffold). The net-shape scaffold is shrunken by controlled drying (dried net-shape scaffold). A secondary treatment is then administered to the dried net-shape scaffold to prevent reswelling when reintroduced into water (heat-treated scaffold). Figure 2 shows an example of the small scale possible with this materials processing strategy.

The goal of this chapter is to develop the material processing strategy, and determine the effects of polymer content and post-processing on dimension, microstructure, and thermomechanical properties of the scaffold.

2.2 Materials and Methods

2.2.1 Materials

Poly(ethylene) glycol diacrylate (PEG-DA) (M_n 700 Da, product no.455008), polyacrylic acid (PAA) solution (50% solution in water, M_W 2000, product no. 535931), and azobisisobutyronitrile (AIBN) (product no. 441090) were purchased from Sigma (St. Louis, MO). Water-based binder (ZB7) was purchased from Zcorp (Burlington, MA). Granulated, white pure cane sucrose (C&H) was purchased from CostCo (Los Angeles, CA). P-dioxane (product no. EM-DX2091-1) was purchased from VWR International. Ethylcellulose (product no. AC190960050) was purchased from Fisher Scientific. Tisseel™ fibrin sealant kits were donated from Baxter Healthcare Corp., BioScience (Westlake Village, CA). Irgacure 2959 (I2959) was donated by Ciba (Basel, Switzerland). Inkjet printheads (Innovera Compatible Remanufactured Inkjet Cartridge for Canon Printer BJC, product no. S5BC20BK) were purchased from Officemax (Naperville, IL).

2.2.2 Preparation, Printing, and Monomer Infusion

Powder Preparation

Granulated, white pure cane sucrose was milled with an analytical mill (Tekmar A-10, Cincinnati, OH) and separated into the desired particle size range of 53-106 μm with stainless steel sieves (W.S. Tyler USA Standard Testing Sieves, Mentor, OH) on a shaker (W.S. Tyler RO-TAP model Rx-29, Mentor, OH) for 30 minutes.

Binder Preparation

A custom binder was made composed of a 2:1 volume ratio of water-based binder and PAA solution (pH 5). Binder composition was previously optimized for preform strength and printing

resolution of sucrose [3]. The binder was filtered with a 0.2 μm polytetrafluoroethylene (PTFE) filter prior to use.

3D Printing

Inkjet printheads were modified to deliver liquid binder in the 3D printer. Briefly, the plastic outer housing and ink pad supplying the reservoir were removed to expose the ink filter above the printhead nozzles. A cross-sectioned 15-mL centrifuge tube was carefully attached over to the ink filter with clear epoxy for a water-tight seal. The tube was filled with the custom binder and primed in a Canon printer (Model BC-20, Canon, Lake Success, NY) before use in the 3D printer (Model Z-402, Z-Corp, Burlington, MA).

3D printer powder bed was loaded with 53-106 μm sucrose particles and the layer thickness set to 0.007". Porogen particle size and layer thickness were previously optimized for preform strength and printing resolution of sucrose [3]. Computer-aided design (CAD) software (Autodesk Inventor, San Rafael, California) was used to create 3D models of the preforms. The 3D models were exported in STL file format for use with the 3D Printer.

For measurement of dimensional changes due to the processing, 5 mm cubic sucrose preforms were printed. To demonstrate the ability to create small features with this process, sucrose preforms with villi-shaped features (cylindrical) were printed in a 2x3 array with dimensions of 1 mm diameter and 2 mm height on a base with dimensions of 1 cm x 1 cm x 3 mm. To demonstrate the ability to use this materials processing strategy for interlocking parts, sucrose preforms were printed with base dimensions of 15 mm diameter and 4mm thickness and cylindrical features 3 mm diameter and 4 mm height. For all samples after printing, the sucrose preforms were dried in the printing bed for 2 hours followed by overnight curing at 80°C.

Lastly, to demonstrate use of a natural polymer to create the net-shape scaffolds, 4 mm diameter and 1 mm tall cylinders were printed.

Polymer Infusion, Polymerization, and Drying

An overall processing scheme is shown in Figure 1. Printed cubic preforms were immersed in monomer solution (PEG-DA (15-40 vol%) and AIBN (1wt%) in p-dioxane) for five minutes and then transferred to a sealed 20 mL scintillation vial for polymerization at 80°C for 40 minutes (n=3 for each condition). After polymerization, the samples were leached overnight at 37°C with multiple water changes to remove the porogen. The net-shape scaffolds were dried at room temperature overnight and then heat treated at 150°C for 75 minutes. The temperature and duration of heat treatment were optimized for dried net-shape scaffolds in pilot studies to prevent reswelling. The heat-treated scaffolds were then reswollen in water overnight to measure retained change in volume. Due to maximum shrinking and maintained porosity after heat treatment seen in 20 vol% PEG-DA scaffolds, this volume of PEG-DA was used in all subsequent experiments.

The preforms with villi-like architecture were processed similarly to the cubic preforms above except for an additional UV polymerization step. These preforms were first immersed in a monomer solution of PEG-DA (20 vol%) and I2959 (1 wt%) in p-dioxane. The infused preforms were exposed to 10 minutes of UV with a UV lamp (Blak-Ray B-100, UVP, Upland, CA) for polymerization at the surface of the features. The samples were then processed same as cubic preforms were described above: immersed in PEG-DA solution (with AIBN), polymerized at 80°C for 40 minutes, and heat treated to retain shrinking (n=3). These additional steps provided shape retention of the high aspect ratio features.

For natural polymer net-shape scaffolds, sucrose preforms were infiltrated with a 5 wt% ethylcellulose in chlorforom solution. The solution was allowed to wick into the preforms for 10 minutes and then dried overnight at room temperature. The sucrose was leached away in water for 2 hours and then dried overnight. The fibrinogen complex component and the thrombin component of the of the fibrin sealant kit were reconstituted without further dilution. The net-shape scaffolds of ethylcellulose were plasma treated for 2 minutes to increase hydrophilicity and then immediately introduced to fibrinogen solution for infiltration. After 10 minutes, the fibrinogen infiltrated ethylcellulose net-shape scaffolds were placed into a pool of thrombin solution at room temperature for 2 hours and then at 4°C overnight to allow for gelation. The entire complex was then placed in chloroform on a shaker plate for 4 hours to remove the ethylcellulose. The fibrin scaffold was washed in water for 1 hour and then dried overnight at room temperature.

2.2.3 Scaffold Characterization

Dimension Measurements

The dimensions of the scaffolds were determined by taking images with a digital microscope (VHX-1000, Keyence, Osaka, Japan) and measuring the dimensions of the features with the software. For cubic samples, the side length was measured four times and averaged for each face. The volume was determined by measuring three separate faces and multiplying the side lengths to determine the volume. For villi-like features, the diameter and length of each pillar was measured four times and averaged for calculation of a cylindrical volume.

Dynamic Mechanical Analysis

The glass transition temperature (T_g) of dried and heat-treated 20 vol% PEG-DA scaffolds was measured via dynamic mechanical analysis (DMA 800, Perkin-Elmer, Norwalk, CT). Dried scaffolds of dimensions 4.5 mm x 3.5 mm x 2 mm were heat treated for varying durations (0, 75, 150, and 300 minutes) at 150°C. The samples were loaded between two non-porous platens and placed under dynamic compression at 0.1 mm displacement and 1 Hz frequency. The loss modulus and storage modulus were determined from -100°C to 200°C at a rate of 5°C/minute. The T_g was determined by the peak tan δ (ratio of loss modulus/storage modulus) of the temperature scan (n=3 for each condition).

SEM Images

Dried and heat-treated scaffolds were sectioned and gold coated with a sputter coater at 20 mA under 70 mTorr for 90 s. Scaffold pore morphology was observed with scanning electron microscopy (SEM, FEI Nova 230 SEM, Hillsboro, Oregon) at 10 kV. Pore size range was determined by measuring SEM images with ImageJ software (National Institutes of Health, Bethesda, MD)

Three-dimensional Microstructural Analysis

Porosity (%) of dried and heat-treated scaffolds was determined by microcomputed tomography (μ-CT). Cylindrical 20 vol% and 40 vol% PEG-DA scaffolds (3.5 mm in diameter, 5 mm in height) were scanned using high resolution μ-CT (SkyScan 1172, SkyScan, Kontich, Belgium) at an image resolution of 5.0 μm (65 kV and 180 mA radiation source) and rotation step of 0.20° (n=3 for each condition). NRecon and CTAn software (SkyScan) were used for volumetric

reconstruction and image analysis. A cylindrical volume of interest with 2.5 mm diameter and 2 mm height (400 images) was selected in the center of the scaffold and applied to all samples for analysis of porosity (%). The threshold was determined by adjusting the minimum threshold until the grayscale images were most accurately represented in the binarized images. An optimal threshold range of 29-255 was applied for all quantitative analysis of μ-CT images.

2.3 Results

2.3.1 Volumetric Shrinkage

2.3.1.1 Effect of monomer percentage on shrinking

All polymer solutions (15-40 vol% PEGDA) successfully polymerized in the interstitial spaces of the cubic sucrose preform. After leaching to remove the porogen, a net-shape scaffold was created and able to maintain its shape after drying at room temperature overnight. Dried net-shape scaffolds decreased in original volume by 92±1.1 vol% at 15 vol% PEGDA, 78±3.1 vol% at 20 vol% PEGDA, 66±2.3 vol% at 30 vol% PEGDA, and 60±3.6 vol% at 40 vol% PEG-DA (Figure 3a). Dried net-shape scaffolds reintroduced to water swelled to similar original volumes except for 15 vol% PEG-DA scaffolds. For 15 vol% PEGDA dried net-shape scaffolds, a decrease in 50 vol% was maintained when reswollen. Reswollen dried net-shape scaffolds had a decrease in original volume by 5.2±3.2 vol% at 20 vol% PEG-DA, 13±12 vol% at 30% PEG-DA, and 11±3.1 vol% at 40 vol% PEG-DA.

2.3.2 Effect of heat treatment on rehydration

A secondary treatment (heat treatment) was administered to the dried net-shape scaffolds to prevent reswelling when reintroduced to water. Heat-treated scaffolds retained shrunken

volumes when reintroduced into water (Figure 3b). Heat-treated scaffolds which were then reswollen in water showed a decrease in original volume of 85±3.1 vol% at 15 vol% PEGDA, 81±4.0 vol% at 20 vol% PEG-DA, 67±4.6 vol% at 30 vol% PEGDA, and 65±4.4 vol% at 40 vol% PEGDA.

2.3.3 Effect of secondary heat treatment on microarchitecture

SEM images of dried net-shape scaffolds show highly porosity for 20-40 vol% PEG-DA before and after heat treatment. 15 vol% PEG-DA dried net-shape and heat-treated scaffolds show much lower porosity and smaller pore size than the scaffolds with larger polymer volumes; this may be due to the lack of stiffness of the 15 vol% PEG-DA scaffolds and subsequent collapse of the microarchitecture during drying. With 20-40 vol% PEGDA net-shape scaffolds, heat treatment does not qualitatively have an effect on the microarchitecture (i.e. porosity and pore size) of the scaffolds as seen in the images (Figure 4). The pore size of 20 vol% PEGDA heat-treated scaffolds ranges from ~9-240 μm.

μ-CT analysis quantitatively shows high porosity for both 20 and 40 vol% PEG-DA dried net-shape scaffolds and no effect of heat treatment on porosity. The porosity for 20 vol% PEG-DA dried net-shape scaffolds before and after heat treatment is 67±2.9% and 64±4.2%, respectively. The porosity for 40 vol% PEG-DA dried net-shape scaffolds before and after heat treatment is 79±3.7% and 76±7.3%, respectively. 3D models representative of 20 and 40 vol% PEGDA dried net-shape scaffolds before and after heat treatment show similar high porosity structures (Figure 5).

2.3.4 Effect of secondary heat treatment time

The effect of duration of heat treatment on T_g of 20 vol% PEG-DA dried net-shape scaffolds was studied with DMA. With increasing heat treatment duration, the T_g of dried net-shape scaffolds increased from -22±3.1°C (0 minutes) to 30±3°C (300 minutes) (Table 1, Figure 6). A secondary peak after T_g was seen in the storage modulus profile at 103±3.9°C for the dried net-shape scaffold before heat treatment (Figure 6).

2.3.5 Fabrication of Villi-like Architecture

Scaffolds mimicking the villi of the small intestine were fabricated at 20 vol% PEG-DA. Villi features of dried net-shape scaffolds decreased from the original volume by 85±3.2 vol% (Figure 7). Heat-treated scaffolds retained a decrease in original volume of 89±2.7 vol% when reintroduced into water. The heat-treated scaffold feature dimensions were 449±44 μm in diameter and 1360±99 μm in height.

2.3.6 Control of Shrinkage

3D interlocking components were designed, printed, and individually processed (Figure 8). After processing, the components were able to fit together.

2.3.7 Natural Polymer Scaffolds

A dried ethylcellulose net-shape scaffold preserved its shape after removal of the sucrose preform material during leaching (Figure 9). The ethylcellulose was then infiltrated with fibrinogen and then fibrin formed in the interstitial spaces with thrombin. After removal of the

ethylcellulose with chlorforom, the resulting fibrin scaffold was able to shrink from drying and retain its cylindrical shape. The qualitative result is seen in Figure 9.

2.4 Discussion

This paper describes a materials processing strategy to increase 3DP resolution by shrinking of a net-shape scaffold. A monomer or polymer solution is infiltrated within the interstitial space of a sucrose preform and polymerized. The porogen and monomer solution solvent is removed by leaching in water. The resulting net-shape scaffold now can shrink by drying due to the large void volume created from porogen removal. A secondary heat treatment retains the shrinkage of the dried net-shape scaffold and the heat-treated scaffold minimally swells when reintroduced to water.

This materials processing strategy provides advantages over direct and indirect 3DP. Polymerization or crosslinking within the interstitial spaces of the preform increase material flexibility [5-8]. There is no need for optimization of binder-powder interaction physics for each material combination as needed for direct 3DP. Polymer-powder combinations which previously were not compatible with consumer grade printhead material (i.e. polymers dissolved in organic solvent) can now be used due to a water-based binder and sucrose powder combination. The selection criteria for materials are monomers or polymers able to polymerize or crosslink in non-aqueous solvents, shrink via drying or external stimuli (i.e. heat or pH), and retain shrinking after a secondary treatment (i.e. heat or additional crosslinking). The use of porogen as the powder in this materials processing strategy provides uniform, high density packing of porogen regardless of complex shapes or internal architecture, a challenge for indirect 3DP. In addition, there are no limitations of shapes or internal architectures due to demolding as in indirect 3DP [1, 9, 10]. The

best resolution from printing water-soluble powder with sucrose was determined it to be ~1 mm after optimizing strength and resolution of the preforms [3]. The materials processing strategy presented in this study can improve resolution to ~500 μm by shrinking.

Shrinking by drying is driven by the capillary tension created in the pores during drying [11]. Briefly, drying in gels is categorized into two stages: constant rate period (CRP) and the falling rate period (FRP) (Figure 10). Liquid evaporates in the CRP at a rate similar to evaporation of liquid from an open dish. As liquid evaporates, liquid moves to cover the surface of the scaffold to minimize the solid-vapor specific energy which is larger than the liquid-vapor specific energy. The liquid in the pores creates a tension which is supported by the solid phase, which therefore goes into compression if compliant. Once the radius of the liquid meniscus is equal to the radius of the pore, the liquid has exerted the maximum force and reaches the critical point. At the critical point, the liquid cannot overcome further stiffening of the network, shrinkage stops, and the drying process now enters the FRP. In FRP, the evaporation of the liquid moves into the interior of the scaffold until all liquid is evaporated without additional shrinkage. As seen in Figure 3, scaffolds with increasing percent volume PEG-DA decreased in amount of shrinking from drying. A stiffer scaffold is able to resist the compression by capillary tension and stop shrinking before a softer scaffold can, resulting in less shrinking.

A secondary heat treatment retained the shrinkage of the dried net-shape scaffold when reintroduced to water. T_g is the temperature at which the material changes from glassy, rigid region to a rubbery, soft region (Figure 11). This transition is due to initiation of micro-Brownian motion of molecular chains from the frozen state with increasing temperature [12]. A secondary tan δ peak (α' peak, ~100°C) seen above than T_g for dried scaffold with no heat treatment may be attributed to T_{ll} relaxation (Figure 5) [13, 14]. T_{ll} relaxation is a transition with

onset of motion of long chain segments or entire polymer chains [15]. This behavior is seen in other materials such as polystyrene [13, 16], polyvinyl chloride, polymethyl methacrylate [14], and polyvinyl alcohol [17]. A critical temperature ($T_{critical}$) above both transitions allows for relaxation of polymer chains to a point where swelling forces cannot overcome the more efficient packing of the polymer chains, causing a sudden decrease in specific volume (Figure 12). This relaxation effect is further evidenced by the trend of increasing heat treatment duration (0 to 300 minutes) with increasing the T_g and storage modulus of the heat-treated scaffolds (Table 1, Figure 6). The increased efficiency of packing polymer chains with increased duration of heat treatment results in the scaffolds becoming stiffer and more difficult to create free volume with micro-Brownian motion (Figure 13). The T_g of dried net-shape scaffolds with 0-300 minute heat treatments are optimally below body temperature. The heat-treated scaffolds are in a rubber-like state *in vivo* and the likelihood of stress fractures to the scaffold when experiencing strains would be reduced compared to a hard, brittle state at a temperature below T_g.

Microarchitecture of dried net-shape scaffolds was qualitatively and quantitatively preserved after heat treatment. SEMs seen before and after heat treatment show similar porosity and pore shape for 20-40 vol% PEG-DA dried net-shape scaffolds (Figure 4). μ-CT scans measured similar high porosity before and after heat treatment. This demonstrates the ability of the heat treatment to create a permanent change in the dried net-shape scaffold which can be then used to preserve the smaller volume even after reintroduction to water.

The ability to tailor and independently vary the scaffold stiffness, peptide chemistry, and peptide concentration makes PEG-DA a desired material to elucidate the effect of these variables on cell behavior in 2D and 3D. There have been many studies using PEG-DA hydrogels with cells (described below) but the shapes are either very simple (i.e. flat slabs) without complex 3D

features or with complex, small features on the 10-100 μm scale in one plane (micro-SLA). The challenge seems to be making a structure with enough stiffness to maintain its shape while incorporating various biofunctionalization modifications such as peptides. Stereolithography (SLA) commonly uses acrylated monomers such as PEG-DA at higher resolutions than with 3DP, however, when peptides are added to the resin to make 3D structures on similar scale to this study, the complexity, number of layers, and resolution of the parts are sacrificed. RGDS added directly to the resin resulted in feature resolutions of ~1 mm [18, 19]. While the surface of the part can be modified after fabrication, a strategy commonly used to coat SLA PPF parts with peptides [20, 21], degradation or erosion of the modified surface would expose inert material. Although this study does not show the incorporation of peptides in the scaffolds, the addition of peptides to PEG-DA with the material processing strategy would most likely be successful and the resolution improved compared to SLA. However, peptide functionality would have to be tested due to a heated secondary treatment.

PEG-DA offers a wide range of stiffness with the same processing. While this study used one molecular weight (MW) PEG-DA to demonstrate this process, stiffer scaffolds can be made with lower MW PEG-DA and softer scaffolds made with higher MW PEG-DA. Stiffness can also be tailored by combining different MW PEG-DA [22]. While storage modulus of the heat-treated scaffold at 20 vol% PEG-DA is 6.5 MPa (Table 1), the optimal mechanical properties of the scaffold depends on the *in vivo* or *in vitro* application. For example, the range of mechanical modulus for hard tissue is 10-1500 MPa and for soft tissue is 0.4-350 MPa [23].

PEG-DA allows for a wide range of biofunctionalizations possible. PEG-DA is commonly biofunctionalized with peptide-containing sequences (i.e. RGD) and modified proteins. RGD and RGDS (i.e. arginine–glycine–aspartic acid-serine) has been widely

incorporated into PEG-DA hydrogels. The peptide sequence is found in cell adhesive domains of fibronectin and interacts with many integrin receptors. RGD-containing sequences have been incorporated into 2D PEG-DA hydrogel studies with porcine valvular interstitial cells [24], human dermal fibroblasts [25], osteoblasts [26], human foreskin fibroblasts [27], and into 3D cell encapsulation studies with hepatocytes [28], human mesenchymal stem cells [29-31], and human embryonic stem cells [32]. Peptides, proteins, and carbohydrates can also be incorporated.

Predictability of shrinkage was demonstrated by designing, printing, and processing components with interlocking positive and negative features (Figure 8). Since individual components can be cultured with cells or biofunctionalized separately before interlocking, interlocking features can be designed for specific spatial control of cell-cell interactions or growth factor presentation. The interlocking parts presented in this study are simple shapes but the materials processing strategy can be used to fabricate much more complicated shapes and create interesting patterns of interaction between multiple parts (i.e. gradients).

A feasibility study was completed to demonstrate the ability to create a shrunken natural polymer scaffold. Two natural polymers were used in this process. First, ethylcellulose was used as a sacrificial material to retain the net shape for the infiltration and formation of fibrin. Fibrin was the final material and shrunken by drying. The ethylcellulose was not verified to be completely removed by chloroform leaching although the fibrin gel subsequently became transparent. The advantage of using a natural polymer as the sacrificial material is that it does not need to be completely removed. Both of these materials are not used in SLA. While SLA materials have expanded toward natural polymers (i.e. alginate and gelatin) through chemical modification [33, 34], both of the materials used in this study have not been used in SLA. A secondary treatment was not applied to the dried fibrin scaffold to prevent reswelling when

reintroduced to water. Further studies are needed to determine the method of additional crosslinking to retain the smaller dimensions.

The limitations of this materials processing strategy are denaturing of heat-sensitive biofunctionalization during heat treatment and incompatibility of polymers in aqueous solutions. The scaffold must be biofunctionalized after heat treatment since the high temperature of heat treatment may denature biological proteins. An alternative is to use a secondary treatment which chemically cross-links the polymer without affecting biological proteins. Direct infiltration of monomer or polymer aqueous solutions would dissolve the preform of sucrose. To use water-soluble materials, the preform would first be coated with a non-water soluble material before infiltration and then the coating removed after polymerization, if necessary.

2.5 Conclusion

A common problem for both direct and indirect 3DP is a limit for resolution due to unavoidable spreading of the binder droplet after contact with the powder. A materials processing strategy to enhance 3DP resolution by controlled shrinking of net-shape scaffolds was demonstrated. This method produced a scaffold with preserved microarchitecture and fixed shrinkage when reintroduced to water. Higher 3DP resolution is now possible with porogen powder.

Acknowledgements

The authors would like to acknowledge Philip Yeranosian, Dr. Armen Derian, and Dr. Min Lee for their guidance and insightful discussions, Dr. Jinny Kwak and Dr. Kang Ting for assistance and use of μ-CT, and Dennis Yuan for assistance in conducting μ-CT scans.

2.6 Tables

Table 1. Increasing heat treatment duration of scaffolds resulted in increased T_g and storage modulus (at 25°C).

	Heat Treatment Duration (min)			
	0	**75**	**150**	**300**
Tg (°C)	-22±3.1	18±0.83	22±1.6	30±3.0
Storage Modulus (MPa)	0.77±0.17	6.5±0.94	8.5±1.3	28±10

2.7 Figures

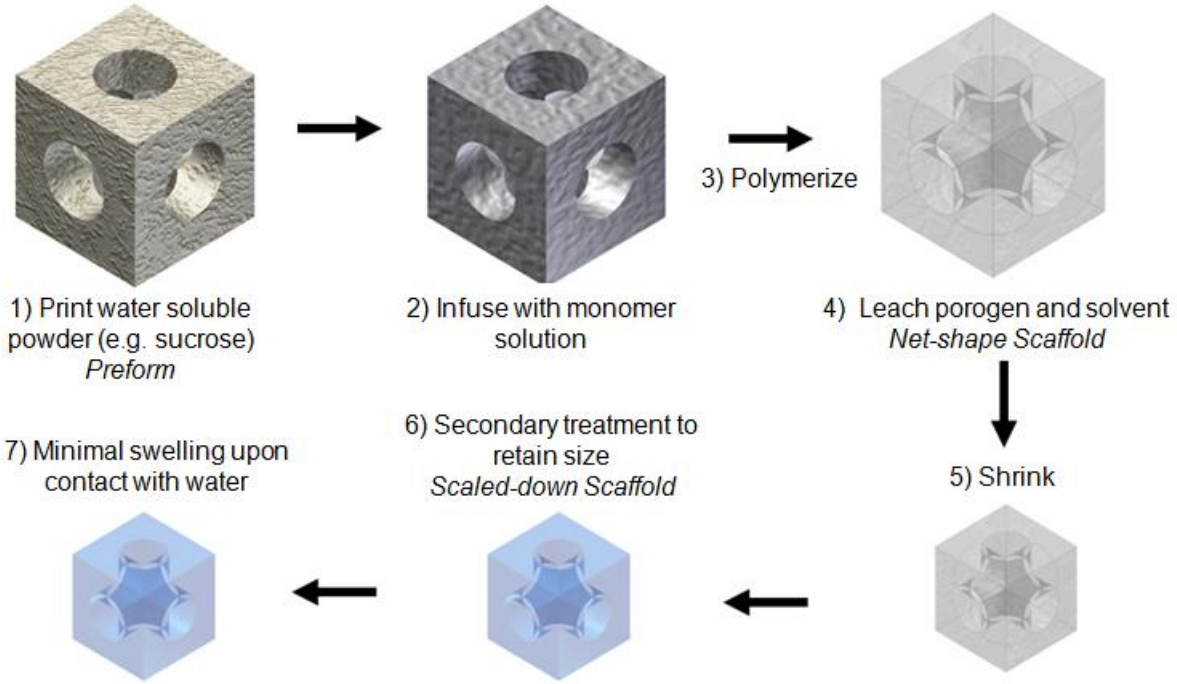

Figure 1. Materials processing strategy to create a net-shape scaffold with fixed shrinkage.

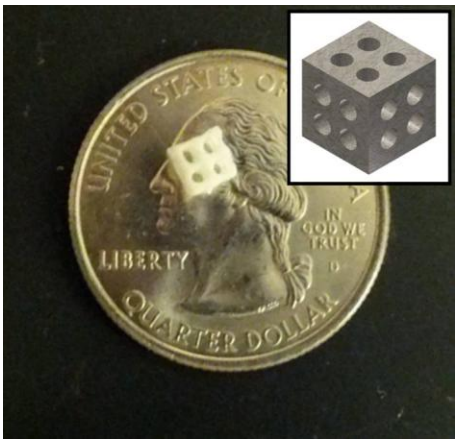

Figure 2. Example of dried net-shape scaffold on a quarter. Inset is design of same structure before processing.

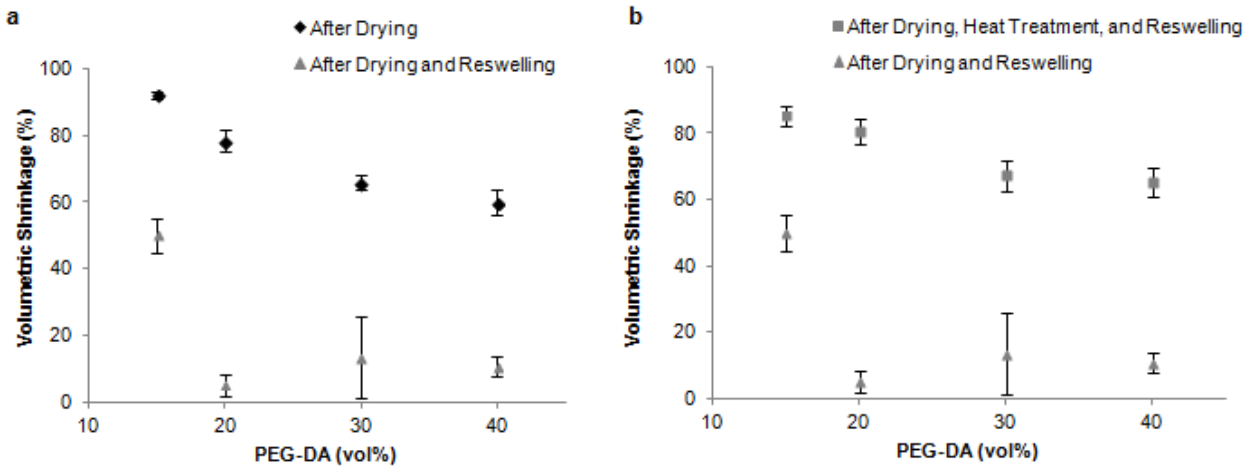

Figure 3. Increasing amount of polymer resulted in decreasing amounts of volumetric shrinkage from drying. Almost complete reswelling to original dimensions was seen for 20-40 vol% PEG-DA except for 15 vol% (a). Dry scaffolds reswollen after heat treatment have retained volumetric shrinkage from drying (b).

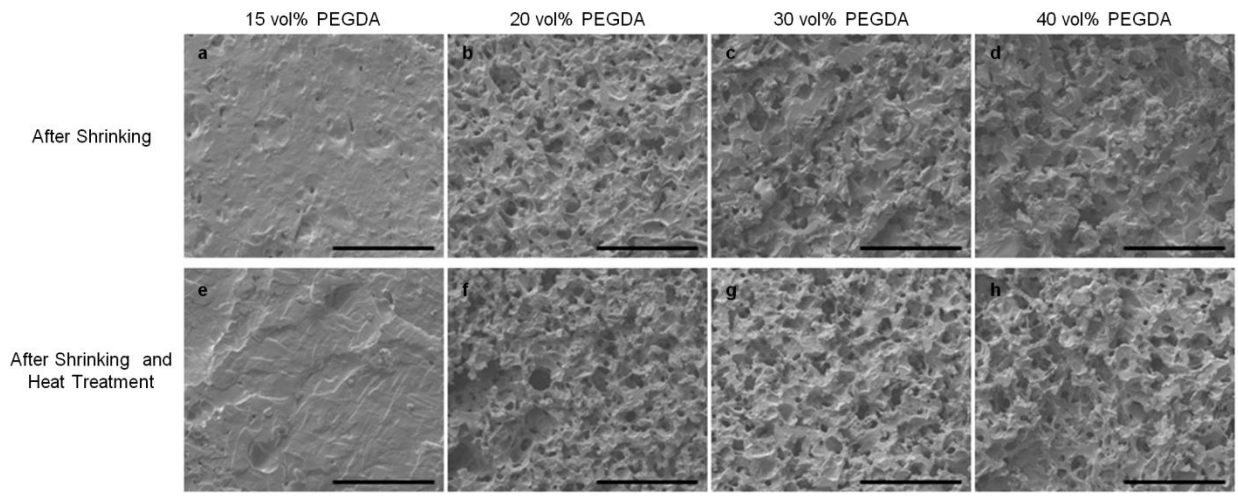

Figure 4. SEM images show preservation of microarchitecture from drying and heat treatment for 20-40 vol% PEG-DA. 15 vol% PEG-DA scaffolds lacked porosity due to collapse of microarchitecture during drying. Scale bar is 300 μm.

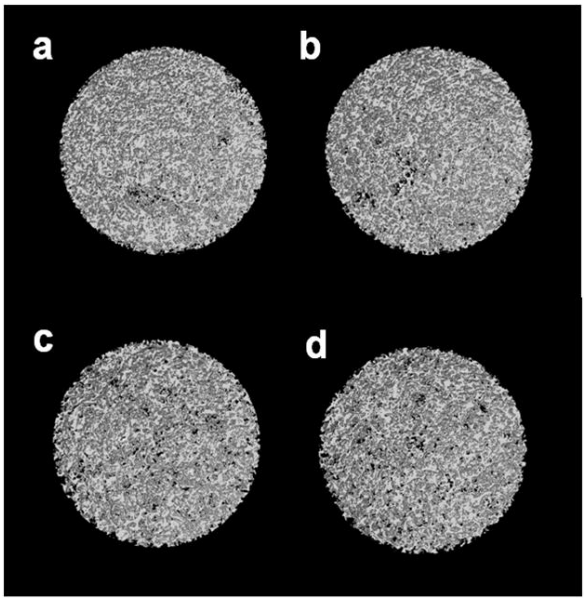

Figure 5. 3D models were constructed from μ-CT images (volume of interest 2.5 cm in diameter and 150 μm thick) show no visible effect of heat treatment on scaffold microarchitecture. The scaffolds are: a) 20 vol% PEG-DA no heat treatment, b) 20 vol% PEG-DA heat treated, c) 40 vol% PEG-DA no heat treatment, and d) 40 vol% PEG-DA heat treated.

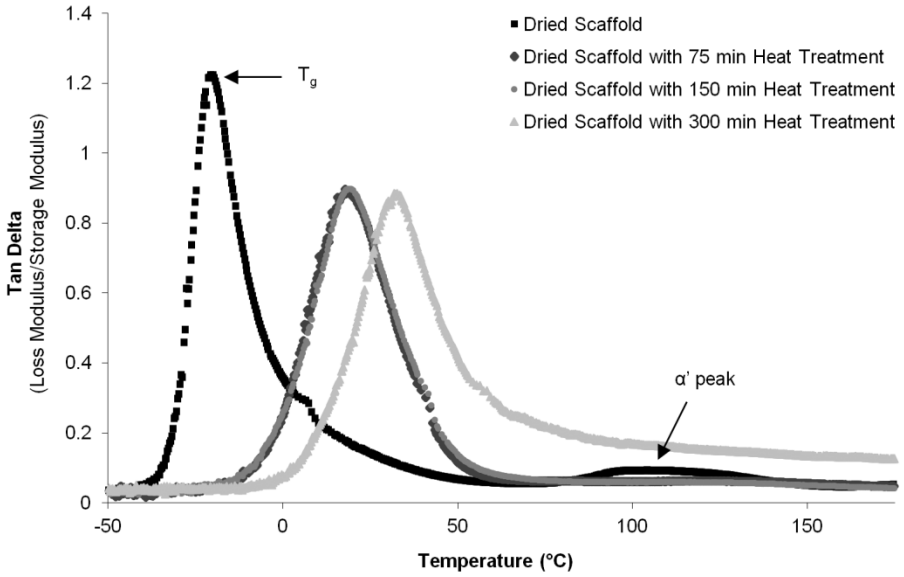

Figure 6. Increased duration of heat treatment resulted in increased T_g as measured by DMA. A secondary peak (α', a pre-melting temperature larger than Tg) is seen for dried scaffolds.

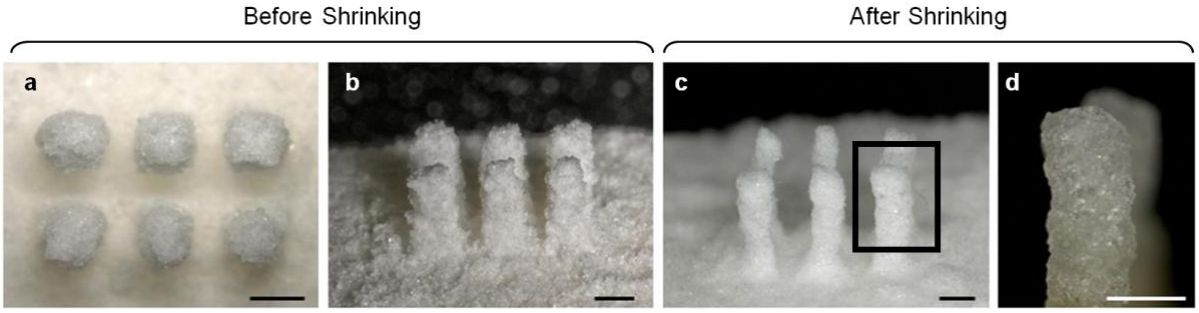

Figure 7. Villi-like features were printed with sucrose (top view, a; angled view, b). Dried scaffolds showed volumetric shrinkage (c). Heat-treated scaffolds retained volumetric shrinkage when reintroduced into water (d). Scale bar for (a) and (b) are 1000 μm, and for (c) and (d) are 500 μm.

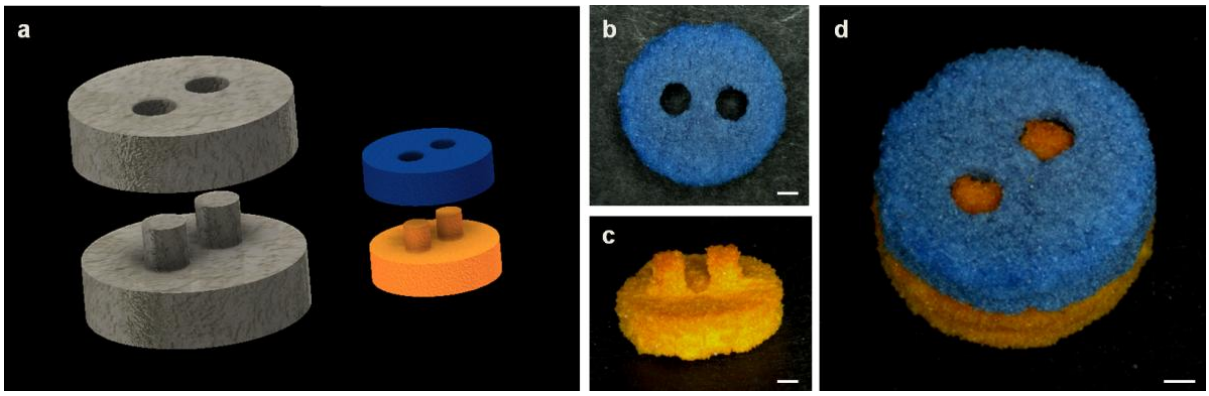

Figure 8. 3D interlocking parts were designed in CAD (a) processed separately (b), and interlocked together (d). Scale bar is 1000 μm.

Figure 9. A feasibility study to show the use of natural polymers for shrinking is shown with an ethylcellulose net-shape scaffold (left) and shrunken fibrin scaffold (right). The ethylcellulose was used as a sacrificial material for the final fibrin scaffold. The dried fibrin scaffold has not been processed with a secondary treatment to retain shrinking. Scale bar is 2 mm.

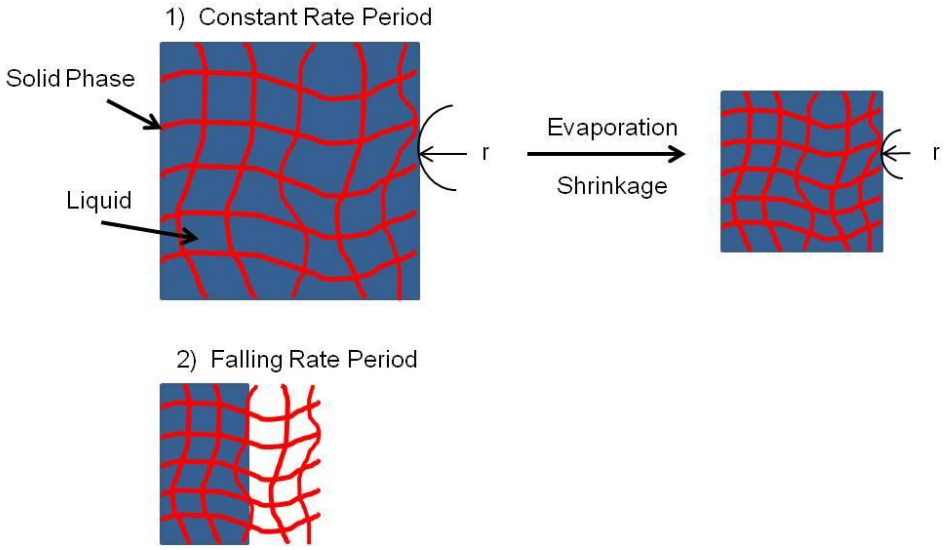

Figure 10. Shrinking of net-shaped scaffolds during drying is driven by capillary tension of the liquid to minimize the solid-vapor specific energy in the constant rate period as liquid evaporates. After the critical point is reached (maximum capillary tension), liquid evaporates within the solid phase.

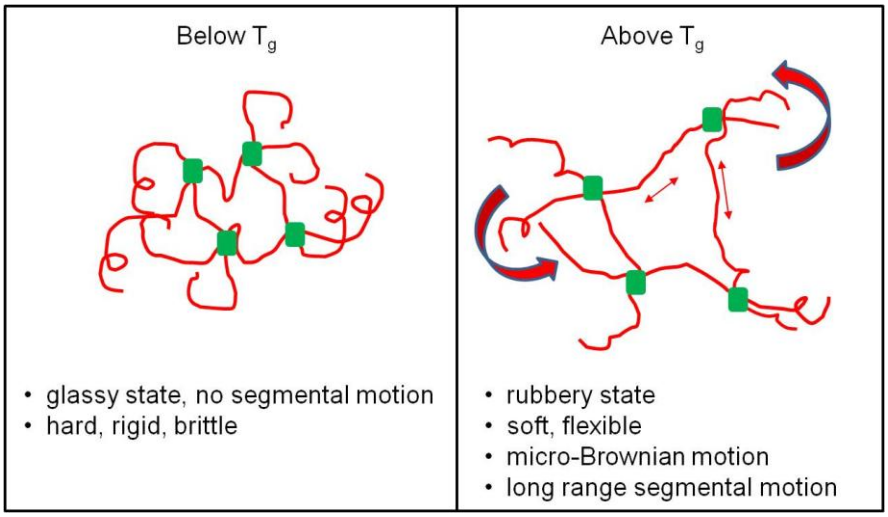

Figure 11. Glass transition temperature ($T_{g)}$ is the temperature at which the material changes from glassy, rigid region to a rubbery, soft region. Below T_g the chains are in the frozen state (left) while above T_g micro-Brownian motion of molecular chains allows for long range segmental motion (right).

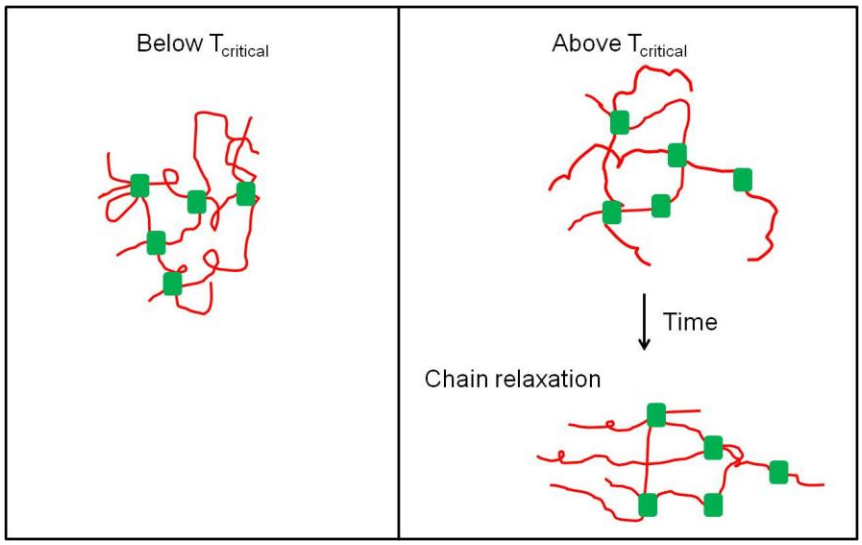

Figure 12. Heating net-shape scaffolds at a critical temperature ($T_{critical}$) above T_g (maximum tan δ) and T_{ll} (α' peak) allows relaxation of polymer chains to a point where swelling forces cannot overcome the more efficient packing of the polymer chains, causing a sudden decrease in specific volume

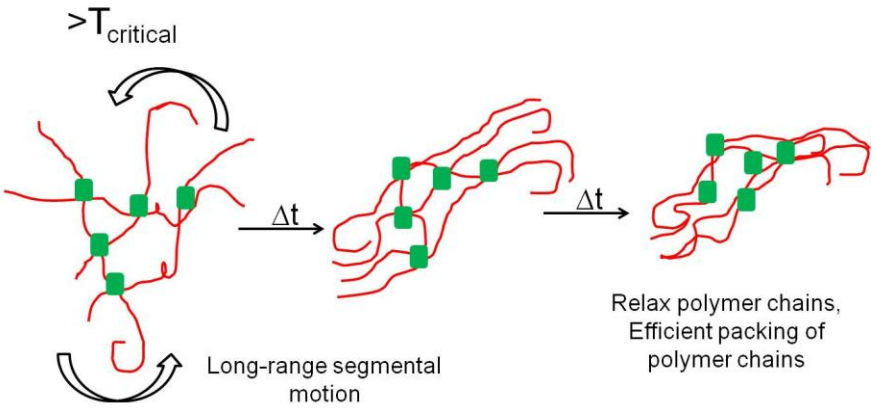

Figure 13. The longer scaffolds are heated at $T_{critical}$**,** the more relaxed polymer chains are with efficient packing of polymer chains.

References

[1] Lee M, Dunn JCY, Wu BM. Scaffold fabrication by indirect three-dimensional printing. Biomaterials. 2005;26:4281-9.

[2] Lee M, Wu BM, Dunn JCY. Effect of scaffold architecture and pore size on smooth muscle cell growth. Journal of Biomedical Materials Research Part A. 2008;87:1010-6.

[3] Yeranosian P, Derian A, Yeranosian M, Wu B. Manuscript in Preparation.

[4] Lee J-Y, Choi B, Wu B, Lee M. Customized biomimetic scaffolds created by indirect three-dimensional printing for tissue engineering. Biofabrication. 2013;5:045003.

[5] Cima MJ, Sachs E, Cima LG, Yoo J, Khanuja S, Borland SW, et al. Computer-derived microstructures by 3D printing: bio-and structural materials. Solid Freeform Fabr Symp Proc: DTIC Document; 1994. p. 181-90.

[6] Wu BM, Borland SW, Giordano RA, Cima LG, Sachs EM, Cima MJ. Solid free-form fabrication of drug delivery devices. Journal of Controlled Release. 1996;40:77-87.

[7] Griffith LG, Wu B, Cima MJ, Powers MJ, Chaignaud B, Vacanti JP. In Vitro Organogenesis of Liver Tissuea. Annals of the New York Academy of Sciences. 1997;831:382-97.

[8] Kim SS, Utsunomiya H, Koski JA, Wu BM, Cima MJ, Sohn J, et al. Survival and function of hepatocytes on a novel three-dimensional synthetic biodegradable polymer scaffold with an intrinsic network of channels. Annals of surgery. 1998;228:8.

[9] Yeong W-Y, Chua C-K, Leong K-F, Chandrasekaran M, Lee M-W. Indirect fabrication of collagen scaffold based on inkjet printing technique. Rapid Prototyping Journal. 2006;12:229-37.

[10] Taboas J, Maddox R, Krebsbach P, Hollister S. Indirect solid free form fabrication of local and global porous, biomimetic and composite 3D polymer-ceramic scaffolds. Biomaterials. 2003;24:181-94.

[11] Scherer GW. Theory of drying. Journal of the American Ceramic Society. 2005;73:3-14.

[12] Murayama T. Dynamic mechanical analysis of polymeric material: Elsevier Scientific Pub. Co.; 1978.

[13] Boyer RF. The relation of transition temperatures to chemical structure in high polymers. Rubber Chemistry and Technology. 1963;36:1303-421.

[14] Ueberreiter K, Naghizadeh J. Thermal diffusivity of polymers. Kolloid-Zeitschrift und Zeitschrift für Polymere. 1972;250:927-31.

[15] Stadnicki S, Gillham J, Boyer R. The Tll (> Tg) transition of atactic polystyrene. Journal of Applied Polymer Science. 1976;20:1245-75.

[16] Gillham JK, Boyer RF. The Tℓℓrelaxation of polystyrene. Journal of Macromolecular Science, Part B: Physics. 1977;13:497-535.

[17] Peppas N. Liquid-state transitions (T> T g) of poly (vinyl alcohol). Colloid and Polymer Science. 1982;260:294-6.

[18] Arcaute K, Mann BK, Wicker RB. Stereolithography of three-dimensional bioactive poly (ethylene glycol) constructs with encapsulated cells. Annals of biomedical engineering. 2006;34:1429-41.

[19] Chan V, Zorlutuna P, Jeong JH, Kong H, Bashir R. Three-dimensional photopatterning of hydrogels using stereolithography for long-term cell encapsulation. Lab on a Chip. 2010;10:2062-70.

[20] Lee JW, Jung JH, Kim DS, Lim G, Cho D-W. Estimation of cell proliferation by various peptide coating at the PPF/DEF 3D scaffold. Microelectronic Engineering. 2009;86:1451-4.

[21] Lan PX, Lee JW, Seol Y-J, Cho D-W. Development of 3D PPF/DEF scaffolds using micro-stereolithography and surface modification. Journal of Materials Science: Materials in Medicine. 2009;20:271-9.

[22] Nguyen QT, Hwang Y, Chen AC, Varghese S, Sah RL. Cartilage-like mechanical properties of poly (ethylene glycol)-diacrylate hydrogels. Biomaterials. 2012.

[23] Hollister SJ. Porous scaffold design for tissue engineering. Nature materials. 2005;4:518-24.

[24] Cushing MC, Liao JT, Jaeggli MP, Anseth KS. Material-based regulation of the myofibroblast phenotype. Biomaterials. 2007;28:3378-87.

[25] Park YD, Tirelli N, Hubbell JA. Photopolymerized hyaluronic acid-based hydrogels and interpenetrating networks. Biomaterials. 2003;24:893-900.

[26] Benoit DSW, Anseth KS. The effect on osteoblast function of colocalized RGD and PHSRN epitopes on PEG surfaces. Biomaterials. 2005;26:5209-20.

[27] Hern DL, Hubbell JA. Incorporation of adhesion peptides into nonadhesive hydrogels useful for tissue resurfacing. Journal of biomedical materials research. 1998;39:266-76.

[28] Underhill GH, Chen AA, Albrecht DR, Bhatia SN. Assessment of hepatocellular function within PEG hydrogels. Biomaterials. 2007;28:256-70.

[29] Salinas CN, Anseth KS. Decorin moieties tethered into PEG networks induce chondrogenesis of human mesenchymal stem cells. Journal of Biomedical Materials Research Part A. 2008;90:456-64.

[30] Salinas CN, Anseth KS. The enhancement of chondrogenic differentiation of human mesenchymal stem cells by enzymatically regulated RGD functionalities. Biomaterials. 2008;29:2370-7.

[31] Nuttelman CR, Tripodi MC, Anseth KS. Synthetic hydrogel niches that promote hMSC viability. Matrix biology. 2005;24:208-18.

[32] Hwang NS, Varghese S, Zhang Z, Elisseeff J. Chondrogenic differentiation of human embryonic stem cell-derived cells in arginine-glycine-aspartate-modified hydrogels. Tissue engineering. 2006;12:2695-706.

[33] Gauvin R, Chen Y-C, Lee JW, Soman P, Zorlutuna P, Nichol JW, et al. Microfabrication of complex porous tissue engineering scaffolds using 3D projection stereolithography. Biomaterials. 2012;33:3824-34.

[34] Zorlutuna P, Jeong JH, Kong H, Bashir R. Stereolithography-Based Hydrogel Microenvironments to Examine Cellular Interactions. Advanced Functional Materials. 2011;21:3642-51.

CHAPTER 3: IMPROVED RESOLUTION OF DIRECT 3D PRINTED SCAFFOLDS BY SHRINKING

3.1 Introduction

A common challenge of both direct and indirect approaches is print resolution due to lateral binder migration [1]. Strategies to minimize binder spreading are introducing a hydrophobic layer on the powder particles [2], improving print head technology to decrease droplet size, or creating macroporous powder particles. Regardless of approaches, there still exists a limit for resolution with these approaches due to unavoidable spreading of the binder droplet after contact with the powder. In this study, the strategy is to increase 3DP resolution by shrinking a direct 3DP print with a plasticizer.

Direct 3DP produces the final part composed of the powder and binder used in fabrication. Materials used in direct 3DP include powder composed of a synthetic polymer (i.e. poly (ε-caprolactone), polylactide–coglycolide or poly (L-lactic acid)) with organic solvent as binder [3-5] and natural polymer powder (i.e.starch, dextran and gelatin) with water as binder [6, 7]. An advantage of direct 3DP is direct control over both the microarchitecture (i.e. pore size) and macroarchitecture (i.e. overall shape). Prints which use porogen as the powder result in high pore interconnectivity, uniform porosity, and defined pore size after leaching. This method has shown to fabricate scaffolds which can support hepatocyte ingrowth [3]. Unlike indirect 3DP, there are no limitations on the macroarchitecture and no need for demolding.

One limitation of direct 3DP is that organic solvents can dissolve polymers used in most printheads. To overcome this limitation, investigators used stencils to pattern polymer solutions onto porogen particles (NaCl) to fabricate scaffolds [3]. However, the use of stencils prevents fabrication of highly complex shapes or small features. Organic solvent-compatible, high precision printheads are available but they are optimized for a narrow range of polymeric

solutions. Another limitation of direct 3DP is that layer thickness must be greater than porogen particle size, and less than 150 μm maximum threshold to maintain interlayer connectivity and part strength during printing [8]. To overcome this porogen size limitation, larger pores must be printed.

Plasticizers are commonly used to increase workability and flexibility of materials to aid in materials processing and are commonly used for pharmaceutical applications [9, 10]. For example, PLA is extremely brittle under tensile and bending loads and a plasticizer such as starch is used to improve processing capabilities [11-14]. In addition to processing capabilities, plasticizers have been used to control degradation time and flexibility of PLGA [15] and PLA [16], drug release kinetics in PLGA microparticles (PEG and TEC) [17] or PLGA films (PEG, [18]; Me-PEG,[19]). PLGA T_g has been shown to be decreased with a range of plasticizers, with triethylcitrate lowering PLGA films made from nanospheres below room temperature [20]. Methanol is a well-known plasticizer (need references) and have been shown to be an effective plasticizer for PMMA [21]. However, methanol has not been reported as a plasticizer for PLGA previously.

An approach to improve 3DP resolution is by shrinking a direct 3DP scaffold. This material processing strategy is shown in Figure 1. Briefly, polymer microparticles are made by emulsion solvent evaporation, washed, collected, and dried. Polymer microparticles are mixed with sucrose particles forming the printing powder. The desired shape is CAD designed and 3D printed by aqueous binder patterned onto the powder in a layer-by-layer fashion to create a 3D print composed of sucrose and polymer. The polymer microparticles are fused together by solvent vapor in an enclosed vessel to create a polymer network. The sucrose is removed by

leaching and then the resulting porous polymer scaffold is shrunken in a solution of 90% methanol overnight. The scaffold is then washed in water and no reswelling occurs.

The goal of this study is to 1) develop a materials processing strategy to increase 3DP resolution and 2) to determine the effect of methanol on volumetric shrinking and glass transition temperature of PLGA scaffolds.

3.2 Materials and Methods

85:15 Poly(DL-lactide-co-glycolide) (PLGA, Inherent viscosity= 0.63 dL/g, product no. B6006-1) was purchased from Lactel (Birmingham, AL). Methanol (histological grade, product no. A433P-4), ethanol (99.5%, product no. AC61509-0010), chloroform (product no C-298-4), and dichloromethane (99.6%, product no 40692) was purchased from Fisher Scentific (Pittsburgh, PA). Polyacrylic acid (PAA) solution (50% solution in water, M_W 2000, product no. 535931) and poly(vinyl alcohol) (average M_w 31,000-50,000, 87-89% hydrolyzed**,** product no. 363073) were purchased from Sigma (St. Louis, MO). Water-based binder (ZB7) was purchased from Zcorp (Burlington, MA). Granulated, white pure cane sucrose (C&H) was purchased from CostCo (Los Angeles, CA). Inkjet printheads (Innovera Compatible Remanufactured Inkjet Cartridge for Canon Printer BJC, product no. S5BC20BK) were purchased from Officemax (Naperville, IL).

3.2.1 Microparticle Fabrication

PLGA microparticles were fabricated using emulsion solvent evaporation. A 2 wt% PLGA in chloroform solution was emulsified in 40 mL of 2 wt% PVA in nanopure water stirred at 450 rpm with a mechanical mixer (Arrow Engineering, Model 6000, Hillside, NJ). The emulsion

was allowed to mix for 1 minute and then 200 mL of 0.5 wt% PVA in water was added. The mixture was allowed to mix for an additional minute. The solution was then moved to a stir plate and magnetic bar added to stir overnight at 400 rpm for the chloroform to evaporate. To wash and collect the microparticles, the solution was centrifuged at 2500 rpm (Eppendorf, Model 5810, Hauppauge, NY) for 5 minutes in 50 mL centrifuge tubes. The supernatant was removed and discarded, 50 mL of nanopure water was added, the centrifuge tube was vortexed to wash the particles, and then centrifuged again. The particles were washed for a total of four times before removing the final supernatant, freezing at -80C, and then lyophilizing overnight to remove any remaining water. The yield was ~87% of the initial amount of PLGA used.

3.2.2. 3D Printing

Powder Preparation

Granulated, white pure cane sucrose was milled with an analytical mill (Tekmar A-10, Cincinnati, OH) and separated into the desired particle size range of 53-106 μm with stainless steel sieves (W.S. Tyler USA Standard Testing Sieves, Mentor, OH) on a shaker (W.S. Tyler RO-TAP model Rx-29, Mentor, OH) for 30 minutes.

Binder Preparation

A custom binder was made composed of a 2:1 volume ratio of water-based binder and PAA solution (pH 5). Binder composition was previously optimized for preform strength and printing resolution of sucrose [2]. The binder was filtered with a 0.2 μm polytetrafluoroethylene (PTFE) filter prior to use.

Printing

Inkjet printheads were modified to deliver liquid binder in the 3D printer. Briefly, the plastic outer housing and ink pad supplying the reservoir were removed to expose the ink filter above the printhead nozzles. A cross-sectioned 15-mL centrifuge tube was carefully attached over to the ink filter with clear epoxy for a water-tight seal. The tube was filled with the custom binder and primed in a Canon printer (Model BC-20, Canon, Lake Success, NY) before use in the 3D printer (Model Z-402, Z-Corp, Burlington, MA).

Computer-aided design (CAD) software (Autodesk Inventor, San Rafael, California) was used to create 3D models of the preforms. The 3D models were exported in STL file format for use with the 3D Printer.

3D printer powder bed was loaded with a 4:1 volume mix of sucrose and PLGA microparticles. The powder was dry mixed by hand thoroughly before use. The layer thickness set to 0.004". The prints were allowed to dry overnight in the bed before removal. To study the effect of solvent and concentration on volumetric shrinking, cylinder shapes were printed with 5.5 mm diameter and 2.5 mm height. A complex 3D shape was designed and shrunken to show shape retention. Thin walls create a honeycomb pattern to form individual cups to hold each cell spheroid. The printed shape had a "cup" diameter 2 mm, wall thickness of 730 μm, "cup" depth of 2.2 mm, and base thickness of 1.4 mm.

3.2.3 Scaffold Fabrication and Shrinking

PLGA microparticles within the 3D print were fused together by placing the 3D print in an enclosed rectangular glass staining vessel with a small crystallizing dish of DCM. The 3D print was not in contact with the DCM. The prints were exposed to DCM vapor for 10 minutes and

then removed from the vessel for 5 minutes. This process was repeated for a total of five times. The fused 3D prints were then placed in water and stirred to leach the sucrose overnight with multiple water changes.

To study the effect of solvent on shrinking, leached scaffolds were placed in 20 mL of different concentrations of methanol, ethanol, or water (i.e. 90% MeOH is 90 vol% methanol and 10 vol% water) in a sealed container overnight at room temperature (n=1). To study the effect of temperature on shrinking, leached scaffolds in water were heated to 35, 45, 55, or 65°C overnight (n=3). Complex shaped prints were shrunken with 90% MeOH overnight at room temperature (n=3). Images were taken before and after solvent or heat treatment to determine dimensions (described below).

3.2.4 Materials Characterization

Imaging

SEM images of the 3D print at each processing step were taken (SEM, FEI Nova 230 SEM, Hillsboro, Oregon) at 10 kV with a low-vacuum detector. The PLGA microparticle size was determined by taking SEM images and measuring the diameter with *ImageJ* software developed at the US National Institutes of Health. The dimensions of 3D prints and scaffolds were measured with a digital microscope and corresponding software (VHX-1000, Keyence, Osaka, Japan).

Differential Scanning Calorimetry

Glass transition temperature (T_g) was determined by differential scanning calorimetry (DSC, PerkinsElmer PYRIS Diamond DSC). Samples of 5-10 mg were loaded and sealed in an

aluminum pan with pinhole. For wet samples, PLGA scaffolds and microparticles incubated with solvent (methanol or ethanol) were tested directly without drying. Excess solution was removed with a Kimwipe to prevent solvent from dripping from the samples. For dry samples, the samples were scanned two times from -60 to 60°C and the T_g determined from the second scan. For wet samples, the samples were scanned once from -20 to 50°C. The heating rate for all scans was 5°C/minute with a dry nitrogen flow of 20 mL/min. The T_g was determined by the midpoint of the baseline shifts associated with c_p of the second scan (n=2 for all conditions).

Polymer Thin Film Fabrication and Testing

For contact angle measurements, a thin film of PLGA on a glass slide was made by spin-coating 0.5 mL of 1.5 wt% PLGA in chloroform solution at 500 rpm for 2 minutes. For DSC experiments, thin films of varying thickness were made by 1, 5, or 15 coats of 0.3 mL of 20 wt% PLGA in chloroform at 400 rpm for 1 minute. Each layer was allowed to dry for 5 minutes before deposition and spin coating of the next layer. The thickness of each sample was measured by SEM of the cross-section. The samples were incubated in methanol overnight and then DSC was performed as described above (n=2 for each thickness).

Contact Angle

The contact angle was determined by recording a video at 60 fps (First Ten Angstroms, FTA32) while a droplet of liquid (water, ethanol, or methanol) was deposited onto the thin film. Images immediately after impact were selected to determine the contact angle with the software (n=3 for all conditions).

Solvent-Cast, Particulate-Leached Scaffolds

Solvent-cast, particulate-leached scaffolds of 85:15 PLGA, PCL, and PLLA were made. Solutions of 8.5 wt% polymer in chloroform were allowed to mix overnight in a sealed scintillation vial. Sucrose particles (53-106 μm, 6.2g) were added to 5 mL of each polymer solution and mixed well before casting in a rectangular teflon mold. After drying overnight, the scaffolds were leached overnight in water at room temperature. The scaffolds were then dried overnight at room temperature and then added to water, ethanol, or methanol. After overnight incubation with these solvents, the scaffolds were compared qualitatively with a picture taken.

3.3 Results

A novel material processing strategy was developed to increase direct 3DP resolution by shrinking. An overview of the process is shown in Figure 1. PLGA microparticles were made by emulsion solvent evaporation with a size range of 16±8 μm in diameter with particle size ranging from 3 to 58 μm. The yield was ~87% of the original weight used in polymer solutions. After lyophilization, the microparticles were in a powder-like state and mixed thoroughly with sucrose particles to create a dry mix. SEM images show smaller PLGA microparticles coating the surface of the sucrose particles (Figure 2a). 3DP structures were successfully printed with PLGA microparticles entrapped between sucrose particles or bound by binder to the surface of sucrose particles (Figure 2b). Periodic exposure of the print to DCM in an enclosed vessel allowed the polymer microparticles to flow and fuse together to form a polymer network (Figure 2c). A total of five cycles of solvent vapor fusion was found to create a polymer network in which the shape was retained after leaching. SEM images after leaching and drying show the network of microparticles and the complete penetration of the solvent vapor for fusion inside of

the print (Figures 3a and b). PLGA scaffolds placed into 90% methanol overnight shrunk, with the exterior and interior of the scaffold exhibiting thicker and smoother polymer structures (Figures 3c and d).

Shrinking was measured with different solvents and at elevated temperatures in water. Methanol was found to be most effective at shrinking PLGA compared to ethanol (Figure 4). PLGA shrinking by methanol was solvent concentration dependent with substantial volumetric shrinking starting at 70% methanol. The maximum volumetric shrinking with methanol was 82% and 88% at 90 and 100% methanol, respectively. Shrinking was retained after overnight reswelling in water with additional volumetric swelling or shrinking to be less than 5% for samples treated with 60-100% methanol solutions (Figure 5). PLGA scaffolds in water were found to shrink at elevated temperatures (Figure 6). There was no shrinking at room temperature. Shrinking increased with increasing temperature above 35°C. Maximum shrinking reached 73±3.9 and 70±1.6% at 55 and 65°C, respectively.

The contact angle of different solvents on a thin PLGA film was measured to determine wettability. The contact angle of water was 85±1.9°, ethanol was 20±1.6°, and methanol was 15±1.2°. Due to extremely fast wetting of ethanol and methanol, the contact angle was determined 0.033 seconds after droplet impact (Table 1).

The T_g of PLGA particles and scaffolds were affected by solvent. The T_g of PLGA in methanol was lower than in ethanol for both particles and scaffolds (Table 2). In methanol, the T_g of scaffolds was higher than of particles at 23±0.3°C and 12±0.5°C, respectively. In ethanol, the T_g of the scaffolds was higher than of particles at 43±1°C and 30±2°C, respectively. The T_g of PLGA without solvent was 48±0.3°C for the polymer directly from manufacturer, 48±0.2°C for microparticles, and 52±0.2 for scaffolds.

Thin films were made with thicknesses of 20, 100, and 267 μm. The samples were plasticized overnight in methanol and the T_g was -13.3±0.7, 4.5±0.1, and 4.6±0.7°C, respectively.

To demonstrate the resolution achievable with this direct 3DP process, a complex shape was designed in CAD and feature size determined before after shrinking in methanol (Figure 7). A concentration of 90 vol% methanol was used for shrinking more complex 3D object since it was found to provide large amounts of shrinkage while maintaining shape. The object design can be seen in Figure 7a. The final thickness of the walls was 412±31 μm (44±2% dimensional shrinkage), channel diameter of 1099±73 μm (46±4% dimensional shrinkage), and thickness of scaffold 1900±62 μm (47±2% dimensional shrinkage). The volumetric shrinkage of the individual cups was 84±4%.

Solvent-cast, particulate-leached scaffolds incubated in different solvents resulted in PLGA scaffolds shrinking in methanol and no other solvents. PCL and PLLA scaffolds showed no shrinking with any solvents (Figure 8).

3.4 Discussion

This paper describes a novel materials processing strategy to increase direct 3DP resolution by shrinking. First, PLGA microparticles are fabricated by emulsion solvent evaporation and then dry mixed with sucrose particles to form the powder for printing. After printing, PLGA microparticles are fused together by solvent vapor in an enclosed vessel. The sucrose is then removed by leaching and PLGA scaffold permanently shrunken ~80% volumetrically in a solution of methanol. The final PLGA scaffold has improved resolution. Four factors were investigated in this study to better understand polymer-solvent compatibility for shrinking: 1)

similarity in Hansen solubility parameters (HSP), 2) wettability of solvent on polymer, 3) solvent diffusion coefficient, and 4) polymer glass transition temperature. To test other polymers, polymer scaffolds of PCL, PLLA, and PLGA were made by solvent cast, particulate leaching and immersed in methanol, ethanol, and water. While the same effect of shrinking in methanol was seen by solvent cast, particulate leached PLGA scaffolds, PCL and PLLA scaffolds did not shrink in ethanol or methanol. Further discussion about each of these four factors important to determine polymer-solvent shrinking compatibility is discussed below.

After printing, polymer microparticles were fused together by repeated exposure of the print to a source of dichloromethane (DCM) in an enclosed vessel (Figure 9). In an enclosed vessel, DCM vaporizes at room temperature and the DCM molecules diffuse toward the polymer microparticle and loosen the coiled shape. The DCM molecules soften the polymer molecules until flow at which time polymer microparticles fuse together to form a thin polymer network. Removal of print from the enclosed system hardens the polymer. Five cycles of 10 minute solvent vapor exposure and 5 minute removal of the print from the vessel to allow re-hardening was found to work extremely well. A one-hour exposure to solvent vapor was found to create too much softening and flow of the polymer microparticles. The extremely thin layer of PLGA produced did not provide enough structural stability to retain shape after leaching. Therefore, the multiple cycles allowed for better control of the flow by slowing it down. After leaching, the net-shape of the original print is preserved. This processing step after printing eliminates the need for organic-solvent compatible printheads and stencils for polymer solution patterns on the powder layers.

This materials processing strategy provides advantages over current direct and indirect 3DP methods. The first advantage of this strategy is the ability to 3DP synthetic polymers

without using organic solvent as the binder, as described above. The second advantage is material flexibility due to incorporating the polymer directly into the powder. During printing, the water-based binder fuses the sucrose particles while entrapping PLGA microparticles and binding polymer particles to the surface of the sucrose particles. The polymer-binder interaction does not need to be optimized for individual polymers since the binder and printing conditions are optimized for sucrose. In addition, there are multiple fabrication methods for creating polymer microparticles including emulsion, coacervation, and spray drying [17]. Lastly, the desired scaffold shape of this materials processing strategy is not limited as in indirect 3DP. In indirect 3DP, there are challenges of uniform porogen packing when filling a mold and of mold removal with complex scaffold shapes. This novel materials processing strategy addresses many challenges in direct and indirect 3DP.

Shrinking improves the current resolution possible with water-soluble porogen. Previously, the best resolution with optimized printing conditions for water-soluble porogen was ~1 mm [2]. The sucrose preform was then subsequently infiltrated with polymer solution to create a scaffold. In this study, the strategy is to improve the resolution by shrinking a direct 3DP scaffold. A solvent (methanol) shrinks by ~80% volumetrically and reaches features of ~400 μm. Physiological features on the hundreds of microns scale can now be reached with this process for direct 3DP.

Shrinking is driven by decreasing the T_g to allow for polymer chain rearrangement and efficient packing of polymer chains (Figure 10). At temperatures below T_g, the polymer chains are frozen and the polymer network is in a solid, brittle state. At temperature above T_g, polymer chains have long-range segmental motion due to micro-Brownian motion and the polymer network is in a rubbery, soft state. The motion of the polymer chain ends and segments increase

the free volume which allows for rearrangement of chains into a more relaxed state. To reduce the T_g below room temperature (for room temperature processing conditions), known plasticizers (alcohols) were used as plasticizing non-solvents. The proposed mechanism of action is seen in Figure 11. First, a polymer network is exposed to the plasticizing non-solvent. With good interaction between the polymer chains and plasticizing non-solvent, the plasticizer molecules diffuse into the polymer network and penetrate between polymer chains. A plasticizer physically intercalates between polymer chains and increases the free volume and decreases T_g. As the T_g of the polymer falls below room temperature, the polymer chains move due to plasticizer molecules acting as lubricant between polymers chains. The long-range segmental motion results in closer packing of the polymer chains, causing shrinking. This mechanism is supported by the results, specifically by the decrease in measured T_g of PLGA in plasticizing non-solvents and the measured changes in volume in the presence of methanol at concentrations above 60%. Volumetric shrinking of PLGA scaffolds by methanol is concentration dependent, with higher concentrations driving more shrinking. Since plasticizer molecules physically sit between polymer chains, lack of shrinkage at lower methanol concentrations is not surprising. At lower concentrations plasticizer molecules may not be physically sitting between enough polymer chains to allow for massive shrinking. Therefore, plasticization of PLGA scaffolds is concentration dependent. Methanol as a plasticizer has been shown with PMMA with induced initial surface swelling and gel formation and then macromolecular reorganization with prolonged exposure [21]. However, large volumetric changes directly driven by a plasticizer have not been reported before.

Four critical factors in plasticizer-driven shrinking of scaffolds were investigated. They are: wetting of plasticizer non-solvent with the solid substrate, diffusion coefficient of the

plasticizer non-solvent in the polymer network, the relative energy difference (Hansen solubility parameters (HSP)), and plasticizer effectiveness. Each factor will be discussed in more detail below.

First, the liquid-solid interaction of the plasticizing non-solvent and polymer network must be favorable. When a droplet of liquid impacts a solid substrate, a high contact angle exhibits strong liquid-liquid interactions since spreading is poor. Liquids with poor wetting become spherical to minimize interaction with the solid surface. A low contact angle exhibits strong solid-liquid interactions and spreading is good. Water has a high contact angle with the PLGA substrate and therefore unfavorable liquid-solid interactions. Both alcohols spread immediately after contact with PLGA films which allows for further interaction of the plasticizer non-solvent molecules and polymer chains. Good wetting between a plasticizing non-solvent and polymer scaffold is critical to allow for the rest of the critical factors to take effect.

Second, the plasticizer non-solvent must be able to diffuse through the polymer network. Although the diffusion coefficient of ethanol and methanol through PLGA is not known, a basic understanding of the difference in diffusion for ethanol and methanol can be inferred from the diffusion coefficient of these alcohols in water. Methanol diffuses faster in water ($D=1.49x10^{-5}$ cm^2/s) than ethanol ($1.23x10^{-5}$ cm^2/s), most likely due to the size difference. The Stokes–Einstein proposed diffusion coefficient is inversely proportional to the radius of the diffusing particle, assuming the particle is spherical. Therefore, a smaller, linear molecule is expected to diffuse faster since the size and shape are more favorable. Although methanol does have a larger diffusion coefficient, the time of diffusion for both alcohols is expected to be similar.

Third, polymer-solvent compatibility is critical and can be predicted by HSP. HSP quantify the dispersion forces (δ_D), dipole-permanent dipole forces (δ_P), and hydrogen bonding

(δ_H) of a substance but do not account for the effect of size and molecular volume. While high solvent-polymer affinity (similar HSP values) would lead to solvation, extremely low affinity would prevent a small molecule to penetrate and pass through it a polymer network. Each substrate or solvent has a point in 3D Hansen space (Figure 12). In Figure 12 we can see the point in Hansen space for the substrate and an interaction radius (R_o) of the substrate (a solvent in Hansen 3D space within this distance will be compatible). The distance between HSP of the substrate and solvent is designated R_a. The relative energy difference (RED) affinity number is an indication of solvent quality for a specific polymer or material and can help predict compatibility [22]. RED is calculated by:

$$R_a/R_o \qquad (1)$$

$$(R_a)^2 = 4(\delta_{D2}-\delta_{D1})^2 + (\delta_{P2}-\delta_{P1})^2 + (\delta_{H2}-\delta_{H1})^2 \qquad (2)$$

where δ_D is the HSP for dispersion forces, δ_P is the HSP for permanent dipole-permanent dipole interactions, and δ_H is the HSP for hydrogen bonding. The HSP of polymers and solvents used in this study and RED calculations can be found in Table 3. RED affinity number below 1 indicates solubility and above 1 indicates immiscibility. In other words, for a solvent to be compatible it must sit in 3D space within the sphere created by R_o. The calculated RED for water is extremely large at 4.2 compared to the RED for methanol and ethanol, 1.7 and 1.3, respectively. While all three solvents do not have a high affinity for PLGA (RED>1), ethanol and methanol have much better solubility than water does. Therefore an appropriate plasticizer has an affinity which is neither too high, leading to dissolution of the polymer, nor too low where the plasticizer cannot come into close contact with and penetrate between the polymer chains.

The fourth factor is plasticizer effectiveness of the non-solvent. Methanol is a much more effective plasticizer of PLGA than ethanol as seen from the larger change in T_g. A good

plasticizing non-solvent must be able to decrease the T_g enough to drive shrinking at room temperature. While ethanol is a plasticizer, it does not have the effectiveness of methanol.

These four critical factors of a plasticizing non-solvent are important in driving shrinking of a polymer scaffold. The non-solvent must be able to come into close contact with the polymer network, diffuse through the network, interact closely with the polymer chains, penetrate between polymer chains, and then plasticize effectively. In choosing a plasticizing non-solvent for other polymers, these four factors should be first determined. In addition, plasticizers other than non-solvents can be used which satisfy these criteria. Possible plasticizers include gases or additives to explore which serve the same function as decreasing the T_g.

Shrinking is irreversible after the plasticizing non-solvent is removed. Reswelling in water causes minimal changes in the volume after methanol treatment. From the SEM images, the polymer network of methanol-treated scaffolds looks more compact with less individual polymer microparticles seen. The polymer chains rearrange during plasticization to a state where reswelling forces of water cannot be overcome. This inelastic deformation allows for high resolution as seen in the two complex 3D shapes presented.

Isotropic shrinking of positive and negative features was seen in this study. The honeycomb-like structure had isotropic shrinking of the negative features (voids or individual "cups") and positive features (walls of the "cups). Isotropic shrinking is challenging since positive and negative features can shrink differently due to their constraints. A negative feature has material surrounding itself while a positive feature is unconstrained except at its base. If the scaffolds did not shrink isotropically, prediction of the shrinking behavior would be critical so that any anisotropy could be compensated for during the CAD process. The isotropic shrinking

seen in this study shows the shrinking method is promising for more complex shapes such as patient-specific shapes.

The difference in T_g of plasticized PLGA microparticles and scaffolds is due to thickness. The diffusion and penetration of the solvent plasticizer through the polymer network may be effected by the characteristic length. The characteristic length of the microparticles is much smaller than that of the scaffolds, a magnitude difference. The T_g of plasticized thin films varying in thickness from 20-267 μm also showed that a thin film corresponded with a lower T_g compared with a film a magnitude thicker. Therefore the effectiveness of the plasticization of the scaffolds is dependent on the thickness of the structure. These samples were incubated only overnight in methanol. A longer incubation time with the plasticizer is expected to allow for complete diffusion of the plasticizer. However, this may not be needed since plasticization reached a minimum amount to drive shrinking of the scaffolds with these studies.

The limitation of this material processing approach is finding the appropriate plasticizer for other polymers. The lack of shrinking by solvent-cast, particulate leached scaffolds of PLLA and PCL by ethanol, methanol, or water shows the importance of proper plasticizer selection. PCL did not shrink because at room temperature it is above its T_g of -60°C. Methanol and ethanol were not effective plasticizers for PLLA (T_g=60-65°C) since the alcohols were only able to decrease the T_g when wet to 57-60 °C. Although these plasticizing non-solvents used in this study did not drive shrinking, there are many plasticizers commonly used in biomedical applications which can be selected [9]. For example, preliminary results show triethyl citrate is also an effective plasticizer for shrinking with 85:15 PLGA scaffolds in water (results not reported). Therefore, effort will need to be investigated in finding an appropriate plasticizer which will decrease the T_g to allow for shrinking. Another strategy to increase material

flexibility is to use the shrunken PLGA scaffold as a sacrificial mold or preform. Since PLGA is biocompatible, complete removal of the material isn't required as a challenge with using sacrificial molds.

Our mechanistic understanding of PLGA with non-solvents applicable to other PLGA and non-solvent processing technologies such as fabricating PLGA micro- or nanoparticles. For example, one method to produce PLGA nanoparticles is to dissolve PLGA in a binary solvent system (e.g. acetone-methanol or acetone-ethanol) and then to add this solution to a PVA solution [27]. The alcohol diffuses to the acetone, the acetone diffuses out of the PLGA particle, and then the particle solidifies. Our mechanism of action which explains the difference between ethanol and methanol in terms of plasticizing ability results in a real difference in particle yield. Our system is also a binary solvent system since remaining solvent (dichloromethane from the polymer microparticle fusion process) in the scaffold interacts with the plasticizing non-solvent. For the making of PLGA nanoparticles, the phase separation rate was found to be increased with increasing alcohol concentrations since the alcohols acted as non-solvents [27]. At 20% alcohol concentration, the yield of ethanol and methanol is ~75% and ~50%, respectively. The difference in yield was verified by the cloud point titration (alcohol percentage at which coacervation of PLGA was generated) with binary solvents containing methanol having a much higher cloud point than binary solvents containing ethanol. From our mechanistic study, the higher plasticizer effectiveness of methanol than ethanol explains the higher concentration of methanol needed to reach coacervation. The close interactions between methanol and PLGA make it harder for methanol to leave the PLGA polymer chains to enter the other solvent. Therefore, this understanding can assist researchers in appropriate selection of non-solvents for maximum yield in PLGA nanoparticle production.

3.5 Conclusion

A direct 3DP materials processing strategy to increase resolution was developed in this study. 3DP PLGA scaffolds were fabricated and methanol was shown to shrink the scaffolds while retaining the shape. The results show methanol is a strong plasticizer by greatly lowering the T_g of PLGA. In addition, methanol has good wettabililty of PLGA on thin films. To investigate the superiority of methanol as the plasticizer by studying the HSP, the determined RED for ethanol is smaller than methanol although both have low affinity. However, the smaller size and less steric hindrance of methanol compared to ethanol is the likely reason methanol to be a more effective plasticizer.

3.6 Tables

Table 1. Polymer-solvent interactions were characterized by measuring contact angle of solvent with PLGA. Contact angles of solvent on PLGA film were measured and showed poor wetting for methanol and ethanol.

Solvent	Contact Angle with PLGA (°)
Water	85±1.9
EtOH	19.5±1.6
MeOH	14.5±1.2

Table 2. T_g of PLGA particles and scaffolds in varying solvents (ethanol, methanol, or water) or states (wet with solvent or dried) determined from DSC.

Structure	Solvent	Wet or Dry	Tg (°C)
Source	None	Dry	48±0.3
Particles	None	Dry	48±0.2
Particles	EtOH	Wet	30±2
Particles	MeOH	Wet	12±0.5
Particles	EtOH	Dry	49±0.8
Particles	MeOH	Dry	49±1.6
Scaffold	EtOH	Wet	43±1
Scaffold	MeOH	Dry	52±1
Scaffold	MeOH	Wet	23±0.3
Scaffold	None	Dry	52±0.2
Scaffold	Water	Wet	47±0.7

Table 3. Material properties of polymer and solvents including HSP and calculated RED.

	Solubility parameter (δ_d, δ_p, δ_h, δ_{total}, $(MPa)^{1/2}$))	Molar Mass (g/mol)	Molar Volume (cm^3mol^{-1})	Relative Energy Difference (calculated) with methanol, ethanol, water, respectively	RED Radius	Tg (°C)
Methanol	15.1, 12.3, 22.3, 29.6 [23]	32	40.7 [23]	---	---	
Ethanol	15.8, 8.8, 19.4, 26.5 [23]	46	58.5 [23]	---	---	
Water	15.5, 16.0, 42.3, 47.8 [23]	18	18 [23]	---	---	
85:15 PLGA	17.4, 8.3, 9.9, 21.7 [24]	----	---	1.7, 1.3, 4.2	8 [24]	48
Poly(L-lactide)	17.6, 5.3, 5.8, 19.3 [25]	---	---	2.2, 1.7, 4.6	8.4 [24]	60-65
Poly (ε-caprolactone)	17, 7.7, 8.3, 20.4 [26]	---	---	3.0, 2.3, 7	5.0 [26]	-60

3.7 Figures

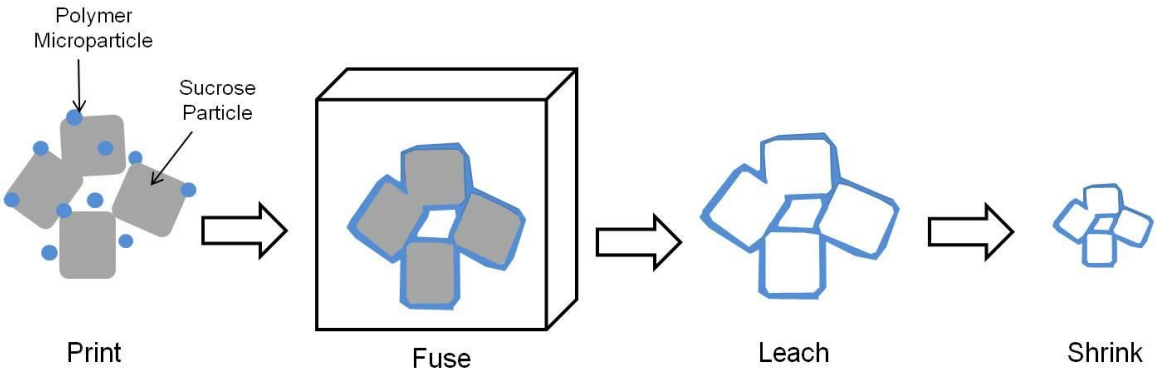

Figure 1. Materials processing strategy for shrinking direct 3DP scaffolds. A dry mix of PLGA microparticles and sucrose particles is prepared as printing powder. The desired shape is printed and then the polymer microparticules are fused together by solvent vapor in an enclosed system. The sucrose is removed by leaching in water and then the scaffold permanently shrunken in 90 vol% methanol.

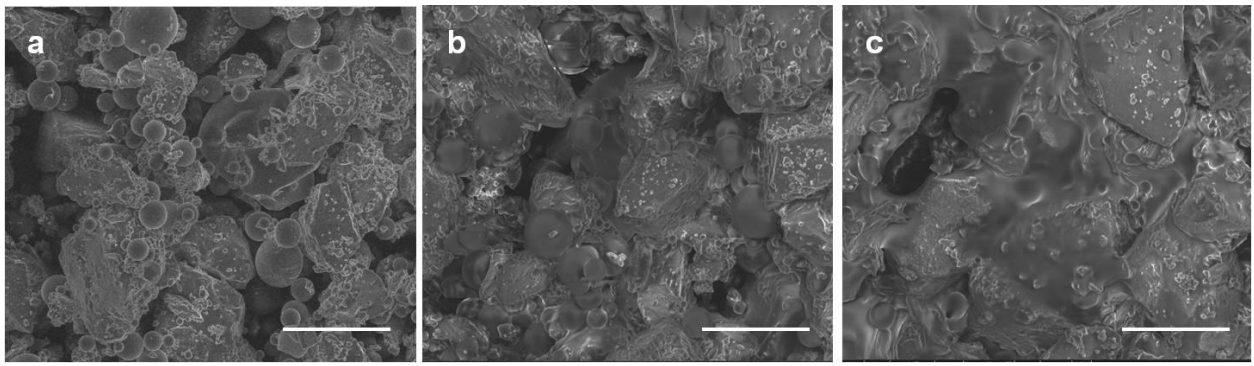

Figure 2. SEM images of PLGA microparticles and sucrose particles in a dry mix (a), bound together by water-based binder during printing (b), and microparticles fused together after exposure to solvent vapor (c). Scale bars are 100 μm.

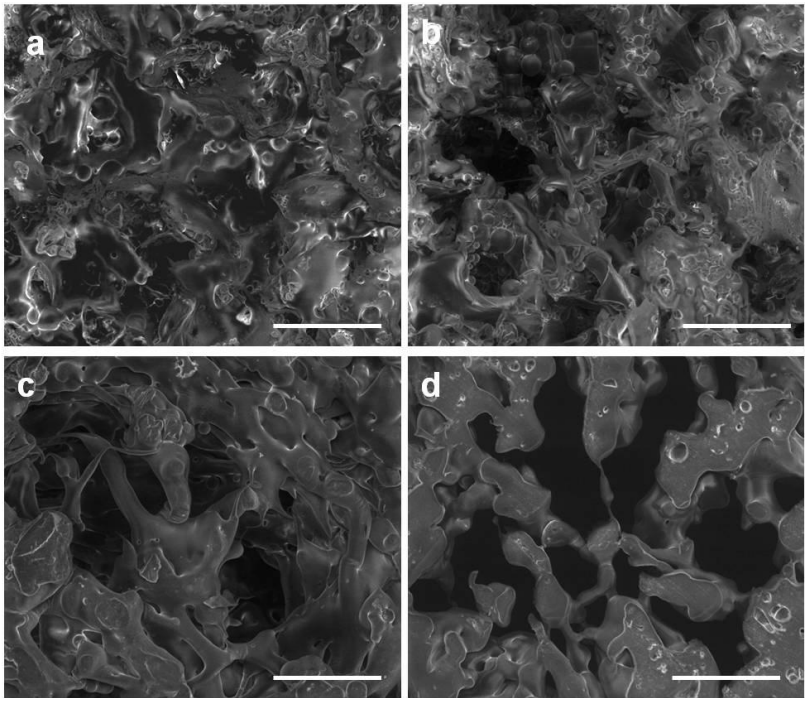

Figure 3. SEM images of dried PLGA scaffolds (exterior (a) and interior (b)) and 90% methanol-treated PLGA scaffolds (exterior (c) and interior (d)). Scale bar is 100 μm.

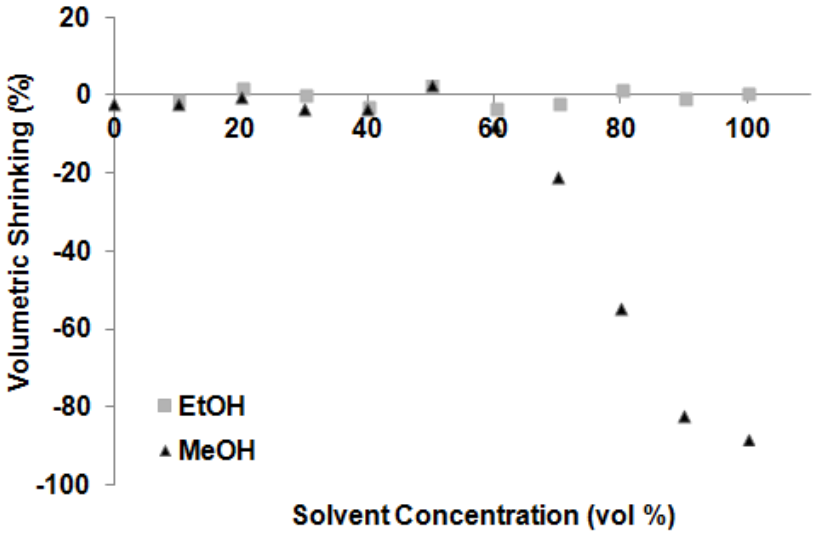

Figure 4. PLGA scaffold shrinking is dependent on non-solvent (methanol or ethanol) and concentration of non-solvent.

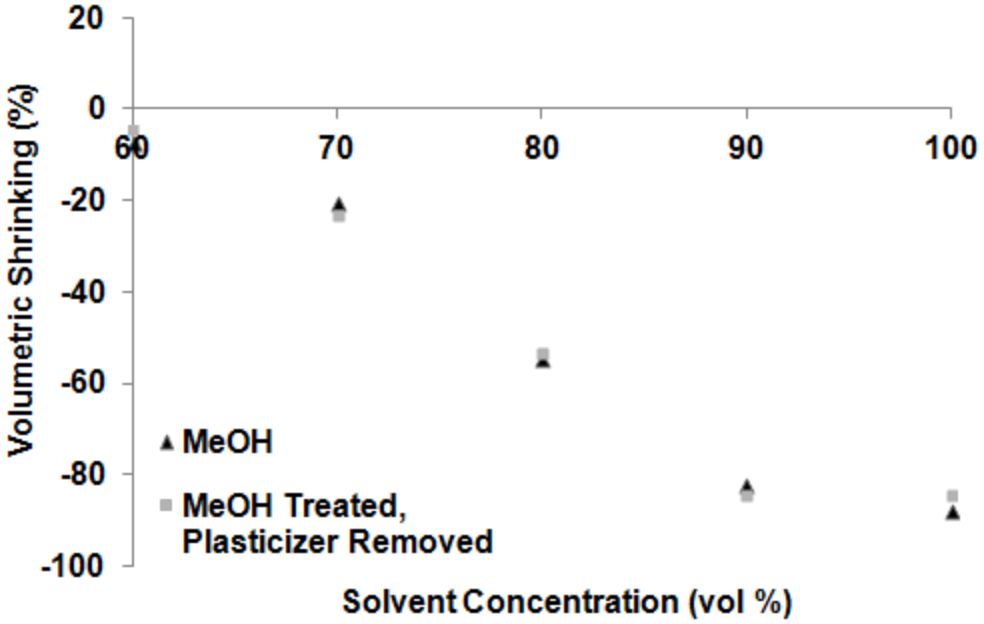

Figure 5. After the plasticizer is removed from MeOH-treated PLGA scaffolds, the PLGA scaffolds maintain the smaller volumes from shrinking.

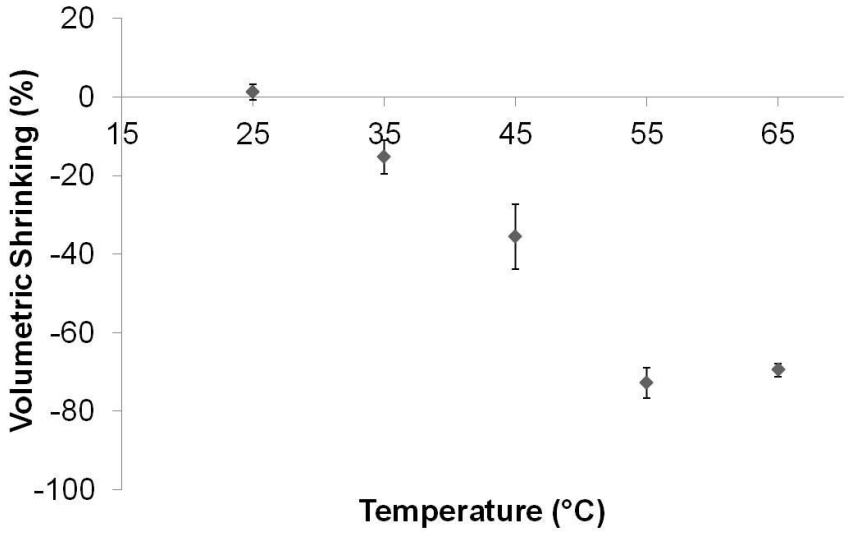

Figure 6. PLGA scaffolds were found to shrink in water by elevating the temperature.

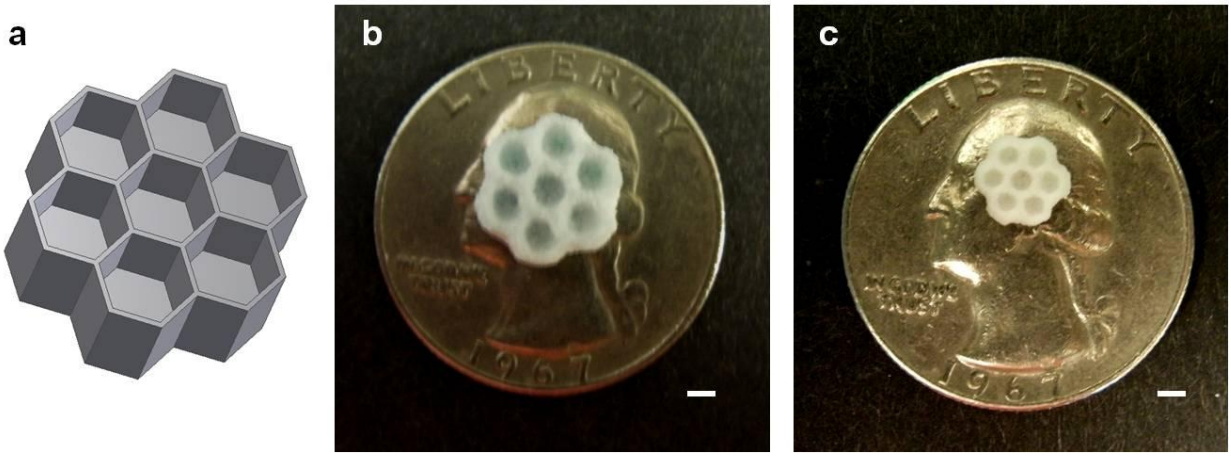

Figure 7. To demonstrate fabricating a stackable 3D spheroid scaffold, a honeycomb-shape was made in CAD (a), 3DP (b), and shrunken by 90% methanol (c). The final scaffold has wall thickness of ~400 μm. Scale bars for b and c are 2 mm.

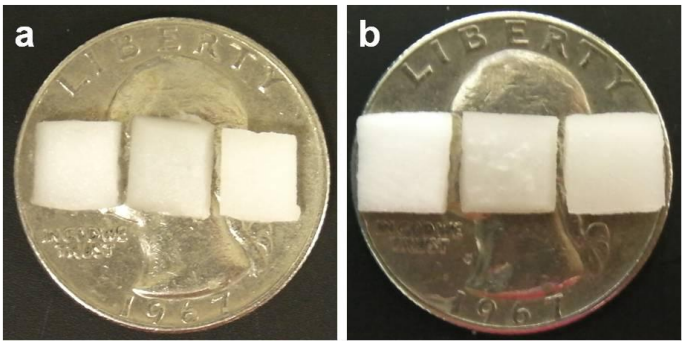

Figure 8. Solvent-cast, particulate-leached PCL (a) and PLLA (b) scaffolds incubated with water, ethanol, or methanol (left to right) did not shrink.

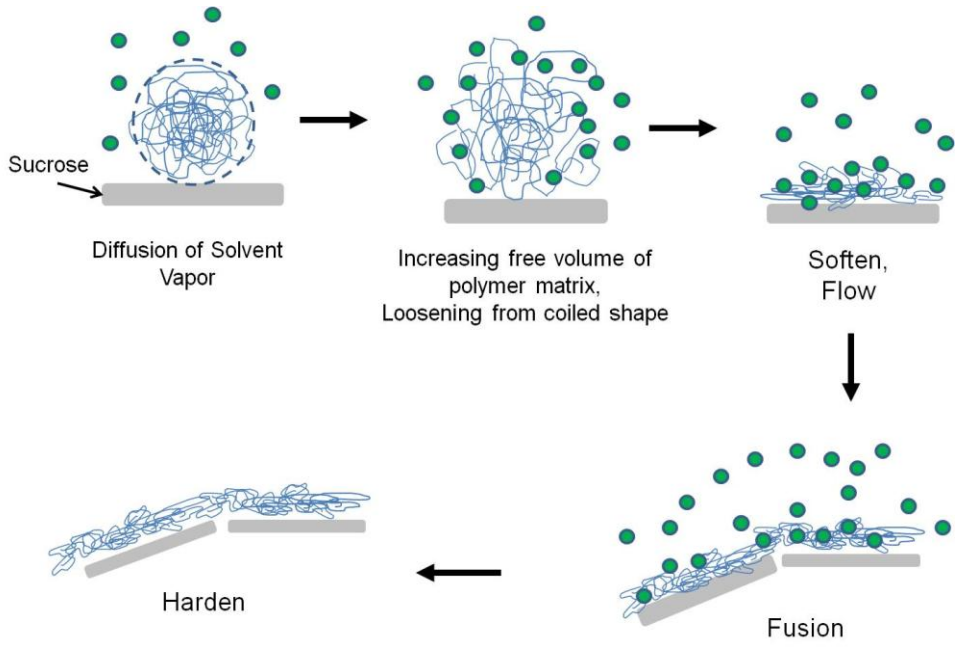

Figure 9. After printing, polymer microparticles were fused together by repeated exposure of the print to a source of dichloromethane (DCM) in an enclosed vessel. In an enclosed vessel, DCM vaporizes at room temperature and the DCM molecules diffuse toward the polymer microparticle and loosen the coiled shape. The DCM molecules soften the polymer molecules until flow at which time polymer microparticles fuse together to form a thin polymer network. Removal of print from the enclosed system hardens the polymer.

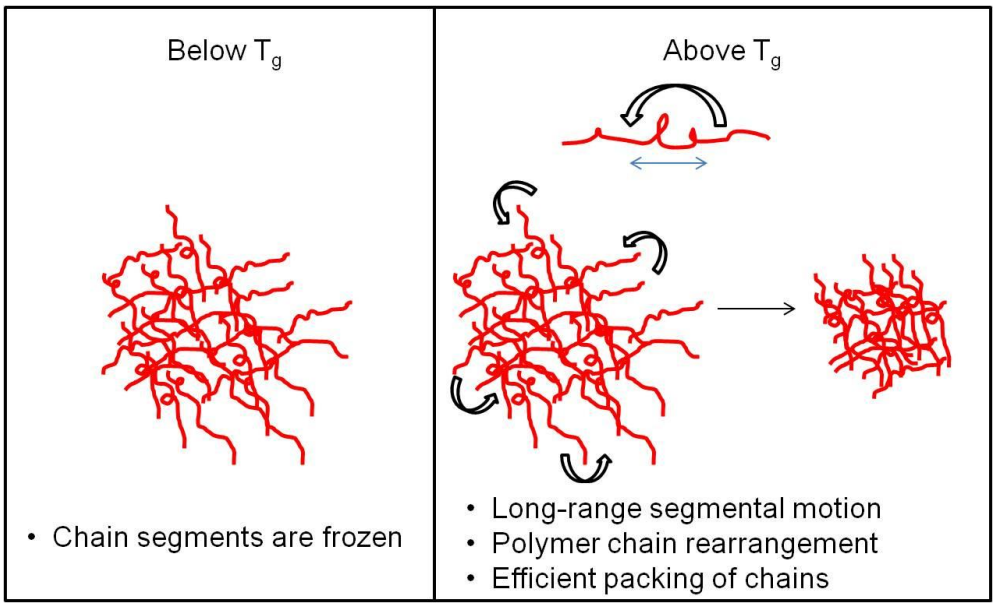

Figure 10. Glass transition temperature ($T_{g)}$ is the temperature at which the material changes from glassy, rigid region to a rubbery, soft region. Below T_g the chains are in the frozen state (left) while above T_g micro-Brownian motion of molecular chains allows for long range segmental motion (right).

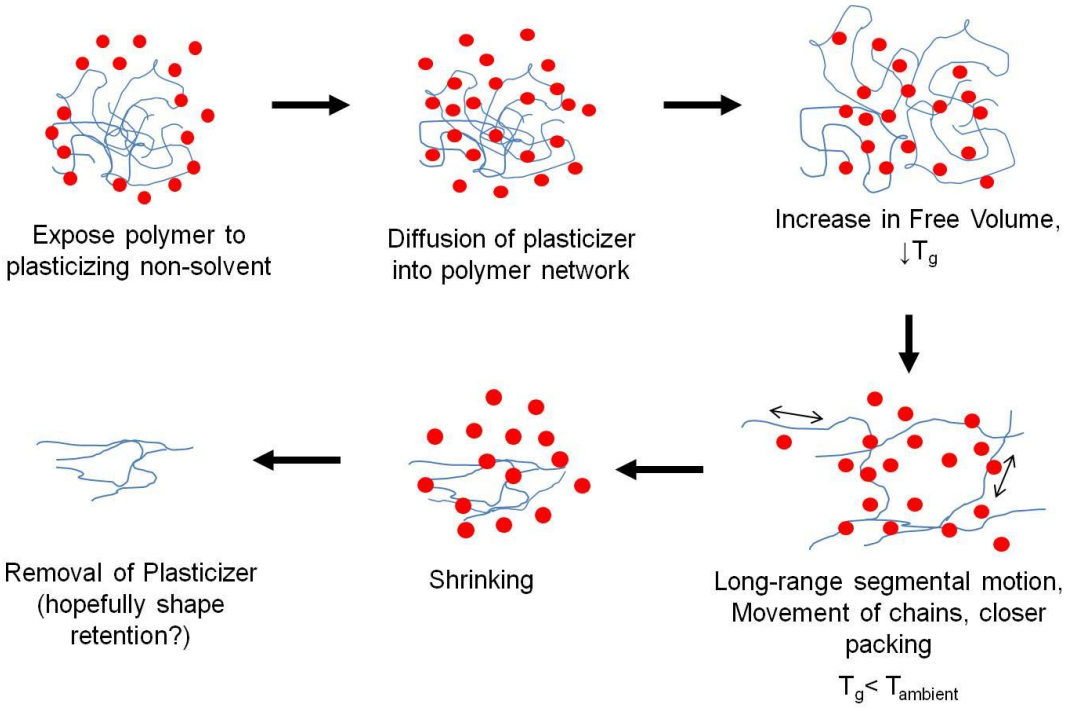

Figure 11. The proposed mechanism of shrinking with a plasticizing non-solvent is first good wetting and affinity of solvent plasticizer on polymer surface. Then the plasticizer non-solvent molecules diffuse through the polymer network and penetrate between the polymer chains, decreasing the T_g. When the T_g is below room temperature, long-range segmental motion allows for closer packing of polymer chains which induces shrinking. Lastly, the shape is retained after removal of plasticizer.

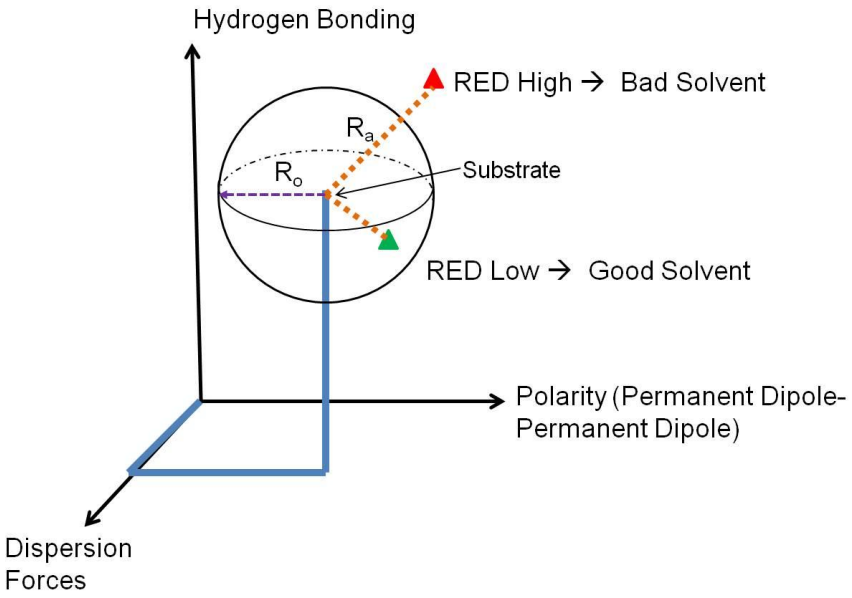

Figure 12. A substrate has a point in 3D Hansen space defined by the HSP. A solvent within the interaction radius (R_o) indicates compatibility while a non-solvent has HSP outside R_o. The relative energy difference (RED) is the distance between the substrate and solvent and indicates solubility (RED<1) or immiscibility (RED>1).

References

[1] Lee M, Dunn JCY, Wu BM. Scaffold fabrication by indirect three-dimensional printing. Biomaterials. 2005;26:4281-9.

[2] Yeranosian P, Derian A, Yeranosian M, Wu B. Manuscript in Preparation.

[3] Kim SS, Utsunomiya H, Koski JA, Wu BM, Cima MJ, Sohn J, et al. Survival and function of hepatocytes on a novel three-dimensional synthetic biodegradable polymer scaffold with an intrinsic network of channels. Annals of surgery. 1998;228:8.

[4] Zeltinger J, Sherwood JK, Graham DA, Müeller R, Griffith LG. Effect of pore size and void fraction on cellular adhesion, proliferation, and matrix deposition. Tissue Engineering. 2001;7:557-72.

[5] Wu BM, Borland SW, Giordano RA, Cima LG, Sachs EM, Cima MJ. Solid free-form fabrication of drug delivery devices. Journal of Controlled Release. 1996;40:77-87.

[6] Lam CXF, Mo XM, Teoh SH, Hutmacher DW. Scaffold development using 3D printing with a starch-based polymer. Materials Science and Engineering: C. 2002;20:49-56.

[7] Seitz H, Rieder W, Irsen S, Leukers B, Tille C. Three-dimensional printing of porous ceramic scaffolds for bone tissue engineering. Journal of Biomedical Materials Research Part B: Applied Biomaterials. 2005;74:782-8.

[8] Wu BM, Cima MJ. Effects of solvent-particle interaction kinetics on microstructure formation during three-dimensional printing. Polymer Engineering & Science. 1999;39:249-60.

[9] Snejdrova E, Dittrich M. Pharmaceutically used plasticizers. Recent advances in plasticizers Rijeka, Croatia: InTech. 2012:45-68.

[10] Mascia L, Xanthos M. An overview of additives and modifiers for polymer blends: Facts, deductions, and uncertainties. Advances in Polymer Technology. 1992;11:237-48.

[11] Jun CL. Reactive blending of biodegradable polymers: PLA and starch. Journal of Polymers and the Environment. 2000;8:33-7.

[12] Martin O, Averous L. Poly (lactic acid): plasticization and properties of biodegradable multiphase systems. Polymer. 2001;42:6209-19.

[13] Jacobsen S, Fritz H-G. Plasticizing polylactide—the effect of different plasticizers on the mechanical properties. Polymer Engineering & Science. 1999;39:1303-10.

[14] Labrecque L, Kumar R, Dave V, Gross R, McCarthy S. Citrate esters as plasticizers for poly (lactic acid). Journal of Applied Polymer Science. 1997;66:1507-13.

[15] Pietro L, Silva DR, do Carmo Alberto-Rincon M, Duek ER. The microscopical characterization of membranes poly (l-glycolic-co-lactic acid) with and without added plasticizer: an in vivo study. Journal of Materials Science: Materials in Medicine. 2008;19:1069-74.

[16] Silva D, Scapin S, Joazeiro P, Alberto-Rincon M, Luciano R, Duek E. In vivo interaction of cells on poly L-(lactic acid) membranes containing plasticizer. Journal of Materials Science: Materials in Medicine. 2002;13:327-32.

[17] Jain RA, Rhodes CT, Railkar AM, Malick AW, Shah NH. Controlled release of drugs from injectable in situ formed biodegradable PLGA microspheres: effect of various formulation variables. European journal of pharmaceutics and biopharmaceutics. 2000;50:257-62.

[18] Wang X, Venkatraman SS, Boey FY, Loo JS, Tan LP. Controlled release of sirolimus from a multilayered PLGA stent matrix. Biomaterials. 2006;27:5588-95.

[19] Owen GR, Jackson JK, Chehroudi B, Brunette DM, Burt HM. An in vitro study of plasticized poly (lactic-co-glycolic acid) films as possible guided tissue regeneration membranes:

Material properties and drug release kinetics. Journal of Biomedical Materials Research Part A. 2010;95:857-69.

[20] Schade A, Niwa T, Takeuchi H, Hino T, Kawashima Y. Aqueous colloidal polymer dispersions of biodegradable DL-lactide/glycolide copolymer as basis for latex films: a new approach for the development of biodegradable depot systems. International journal of pharmaceutics. 1995;117:209-17.

[21] Briscoe B, Pelillo E, Ragazzi F, Sinha S. Scratch deformation of methanol plasticized poly (methylmethacrylate) surfaces. Polymer. 1998;39:2161-8.

[22] Hansen CM. Aspects of solubility, surfaces and diffusion in polymers. Progress in organic coatings. 2004;51:55-66.

[23] Hansen CM. Hansen solubility parameters: a user's handbook: CRC press; 2007.

[24] Schenderlein S, Lück M, Müller B. Partial solubility parameters of poly (D, L-lactide-co-glycolide). International journal of pharmaceutics. 2004;286:19-26.

[25] Agrawal A, Saran AD, Rath SS, Khanna A. Constrained nonlinear optimization for solubility parameters of poly (lactic acid) and poly (glycolic acid)—validation and comparison. Polymer. 2004;45:8603-12.

[26] Bordes C, Fréville V, Ruffin E, Marote P, Gauvrit J, Briançon S, et al. Determination of poly (ε-caprolactone) solubility parameters: Application to solvent substitution in a microencapsulation process. International journal of pharmaceutics. 2010;383:236-43.

[27] Murakami H, Kobayashi M, Takeuchi H, Kawashima Y. Further application of a modified spontaneous emulsification solvent diffusion method to various types of PLGA and PLA polymers for preparation of nanoparticles. Powder technology. 2000;107.1: 137-143.

CHAPTER 4: CONCLUSIONS AND FUTURE DIRECTIONS

4.1 Conclusions

This dissertation reports research addressing the need for strategies to improve 3DP resolution. Instead of optimizing printing conditions (i.e. viscosity and composition of binder, particle size, etc), the strategy presented in these studies was shrinking to attain higher resolutions.

A materials processing strategy was presented for indirect 3DP in Chapter 2. For indirect 3DP, a water-soluble preform was printed and then infiltrated with a final material choice. While the material was crosslinked with heat-initiated polymerization, the advantage of this approach is the ability to crosslink without use of only UV as stereolithography is limited to. Material flexibility is retained since materials with physical or chemical crosslinking can be used with this materials processing strategy. Shrinking was driven by drying in this study and, therefore, a secondary treatment was required to retain the smaller dimensions when reintroduced to water. Small features with controlled shrinking were demonstrated with shrinking of 80 vol%.

A novel direct 3DP fabrication method and materials processing strategy was presented in Chapter 3. PLGA microparticles were fabricated and then dry mixed with sucrose particles to create the printing powder. During printing, the polymer microparticles are trapped within the print between sucrose particles or bound to the surface of sucrose particles by the water-based binder. The particles were then fused after printing by solvent vapor, creating a polymer network which retains the printed shape. Lastly, irreversible shrinking of the PLGA scaffolds was driven by using a plasticizer—methanol. Shrinking by 80 vol% has reached resolution of ~400 μm. Characterization of polymer-solvent compatibility for shrinking led to factors important for plasticizer selection.

4.2 Future Directions

For indirect 3DP shrinking, additional secondary treatments should be developed for application to other materials. While shrinking is a great strategy to reach higher resolutions, a secondary treatment will be needed to prevent reswelling when introduced into water. For natural polymers, additional crosslinking can be investigated. In addition, other materials can be investigated which shrink due to external stimuli. There are polymers which may shrink due to external stimuli (i.e. temperature or pH) and would be interesting to explore for this materials processing strategy.

For direct 3DP, application of the novel direct 3DP materials processing strategy to other polymers would be extremely interesting. The most challenging part would be to select an effective plasticizer to drive shrinking. Four factors were identified and studied in Chapter 3 including HSP and change in T_g. Future work can characterize and study additional factors which may affect plasticizer-polymer compatibility and determine the importance of each factor. With this information, plasticizer selection will be more accurate and faster.

If a plasticizer is not completely effective, other strategies can be used in addition to the plasticizer to drive shrinking. Strategies such as elevating the temperature slightly or adding an internal plasticizer can help the overall system favor shrinking. Therefore this further work would increase the candidate plasticizers if one of the factors is not completely compatible.

Lastly, since polymer microparticles are fabricated prior to printing, this direct 3DP process can be tried with polymer microparticles embedded with drugs or proteins of interest. There are many polymer microparticles of different formulations and shapes used for drug delivery; it would be very interesting to make them into scaffolds for *in vitro* or *in vivo* applications.